A GEOPHYSICAL CHARACTERIZATION OF STRATIGRAPHY IN THE EASTERN BLACK WARRIOR BASIN UNDERLYING GORGAS POWER GENERATION PLANT, WALKER COUNTY, ALABAMA

by

RACHAEL SHEA RUTTER

ANDREW M. GOODLIFFE, COMMITTEE CHAIR

DELORES ROBINSON
SAMANTHA HANSEN
JACK C. PASHIN

A THESIS

Submitted in partial fulfillment of the requirements
for the degree of Master of Arts
in the Department of Geological Sciences
in the Graduate School of
The University of Alabama

TUSCALOOSA, ALABAMA

2012

ABSTRACT

The Black Warrior Basin is a triangular shaped foreland basin located in the southeastern United States between the Appalachian and Ouachita fold and thrust belts. The basin has the potential to provide geologic carbon sinks into multiple stacked saline reservoirs over a large area. CO_2 storage potential of saline aquifers and oil and gas reservoirs in the Black Warrior Basin has yet to be fully assessed. This study evaluates saline reservoirs on the eastern edge of the basin underlying William C. Gorgas Power Plant (Plant Gorgas), Walker County, Alabama. Key reservoirs include the Pennsylvanian Boyles Sandstone, the Mississippian Hartselle Sandstone and Tuscumbia Limestone, and the Ordovician Stones River Group. Data include two post-stack time-migrated seismic reflection profiles, geophysical logs collected in a 1498 m (4915 ft) stratigraphic test well, and a zero-offset vertical seismic profile (ZVSP). Interpretations of key seismic reflectors in the Black Warrior Basin are presented based on a synthetic seismogram, check-shots, a zero-offset VSP, and a well-constrained well-seismic tie. Units in the velocity model are based on lithologic boundaries interpreted as seismic horizons and well tops. An investigation of geologic structures and the lateral extent of saline aquifers in the area surrounding Plant Gorgas is based on depth converted seismic data. Volumetric calculations for the Boyles and Hartselle sandstones, and the Tuscumbia and Stones River Group limestones were calculated to demonstrate the potential to store substantial amounts of carbon dioxide in the Black Warrior Basin. The volumetric estimations that are listed below show the effects of injecting 10% of Plant Gorgas's

emissions (0.75 Megatons of CO_2/year) over a thirty-year period. The Lower Boyles Sandstone CO_2 plume would extend to a radius of 3.6 km (2.25 miles) ± 0.22 km (0.14 miles) around the borehole; 5.2 km (3.23 miles) ± 0.35 km (0.22 miles) in the Hartselle Sandstone; 4.7 km (2.92 miles) ± 0.07 km (0.04 miles) in the Tuscumbia Limestone; and 7.2 km (4.47 miles) ± 0.065 km (0.04 miles) in the Stones River Formation.

DEDICATION

This thesis is dedicated to my grandparents, Ed and Nell Wall. Without them I would not be where I am today. They have supported me throughout my life and I am ever grateful to them for their graciousness.

LIST OF ABBREVIATIONS AND SYMBOLS

ms	Milliseconds
m	Meters
ft	Feet
twt	Two-way time
owt	One-way time
VSP	Vertical Seismic Profile
ZVSP	Zero-offset vertical seismic profile
BWB	Black Warrior Basin
<	Less than
=	Equal to
Φ	Phi – Porosity
ITO	Intelligent Take-out Interval
DGF	Digital Grouped Formation
PR	Point receiver
GAC	Geophone Accelerometer
VSI	Versatile Seismic Imager

ACKNOWLEDGMENTS

I am pleased to have this opportunity to thank the many colleagues, friends, and faculty members who have helped me with this research project. I am most indebted to Andrew Goodliffe, the chairman of this thesis, for sharing his research expertise. I would also like to thank all of my committee members, Delores Robinson, Jack Pashin, and Samantha Hansen for their invaluable input, inspiring questions, and support of both the thesis and my academic progress. I would likely to solely acknowledge Jack Pashin for sharing his expertise on all things Black Warrior Basin. I would like to thank Whitney Harris for helping me with geophysical applications and taking the time to explain them thoroughly.

This research would not have been possible without the support of my friends and fellow graduate students and of course my family who never stopped encouraging me to persist. I would also like to acknowledge my best friend and boyfriend Lance Wilson, who has always been by my side and knew just what to say to motivate me to finish this thesis.

This project was supported through an American Recovery and Reinvestment Act grant issued by the Department of Energy and the National Energy Technology Lab. I also acknowledge generous support through The University of Alabama Department of Geological Sciences.

CONTENTS

LIST OF TABLES

LIST OF FIGURES

1.0 INTRODUCTION

The Black Warrior Basin extends from North Central Alabama to North Central Mississippi and covers an area of 59,000 km^2 (23,000 $miles^2$; Ryder, 1987; Figure 1). The basin is a triangular sedimentary catchment that formed as a foreland basin adjacent to the orogenic syntaxis of the Ouachita (to the southwest) and Alleghanian (to the east and southeast) fold and thrust belts during the Late Paleozoic (Thomas, 1988; Thomas and Whiting, 1994; Pashin, 1994). The Nashville dome marks the northern forebuldge boundary of the basin.

A stratigraphic characterization of the basin is conducted to determine the capacity and injectivity of reservoirs in the Black Warrior Basin surrounding Plant Gorgas. The plant is located on gently dipping stratum that bounds the Alleghanian thrust system west of the Sequatchie Anticline that has been attributed by some as being the western-most limit of thrusting. Deep saline aquifers and oil and gas reservoirs could hold the largest volumes of CO_2 in comparison to the other types of lithologic units with storage potential (Bachu et al, 2004; Esposito et al, 2008). The primary targets for this study are stacked saline aquifers of the Boyles Sandstone, the Hartselle Sandstone, the Tuscumbia Limestone, and the Stones River Group Limestone. Their storage potential is characterized using depth, thickness, and porosity of formations underlying Plant Gorgas. Capacity estimates for the Black Warrior Basin are expected to be on the scale of gigatons (Clark and Pashin, 2009). This amount of storage could provide long term emission disposal until cleaner forms of energy are readily available.

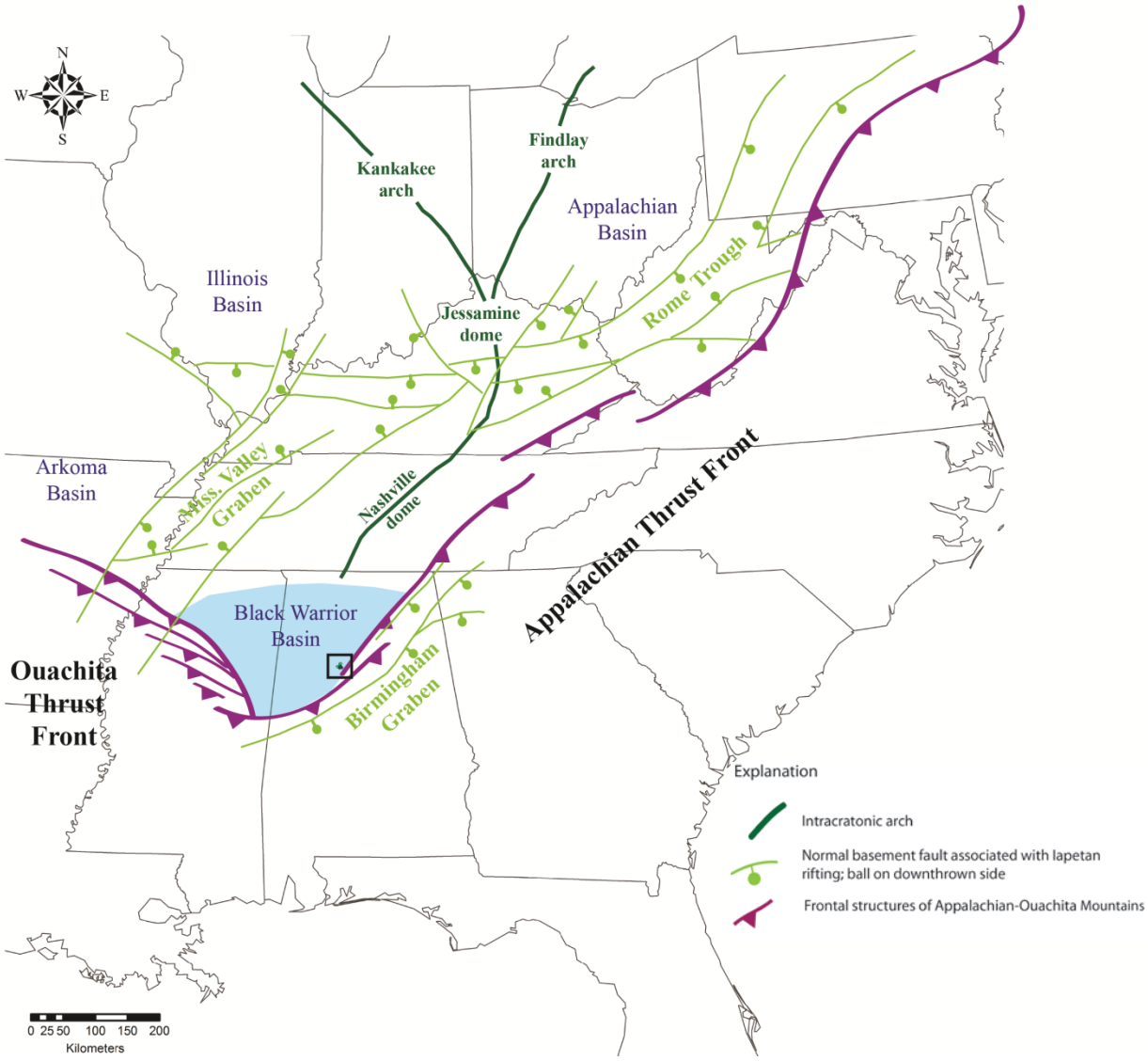

Figure 1: Tectonic map showing the location of the Black Warrior Basin (blue shaded region) in relation to the Ouachita and Alleghanian thrust belts (purple), the regional graben systems (light green), and the domes (dark green; Thomas, 1988; Thomas, 1994; Pashin, 2011).

Two coal fired electricity generation plants, William C. Gorgas (7.53 Megatons (Mt) emitted annually) and James. H. Miller, Jr. (19.92 Mt emitted annually), are located 5 miles apart on the eastern margin of the Black Warrior Basin in Walker County, Alabama (Figure 2). Plant Miller is larger, newer, and a more suitable candidate for carbon capture because it could be more easily retrofitted. However, this plant is located on a ramp of a large fault bend fold structure, the Sequatchie Anticline, and has a greater risk of fracturing in the subsurface which could create leakage pathways. Plant Gorgas is located to the west of the anticline where there is less structural complexity. The thrust fault that carries the Sequatchie Anticline is exposed to the northeast of the characterization site, but the anticline plunges to the southwest, away from Plant Gorgas and ends in a blind termination (Thomas and Bayona, 2002; Figure 1) east of the site.

To be considered for permanent sequestration, formations must have porosity and permeability, similar to a conventional oil and gas reservoir. Reservoirs should be permeable enough for the CO_2 to travel outwards from the borehole to accommodate large injection quantities (Kaldi et al, 2009) and preferably deeper than 755.9 m (2480 feet) so pressure keeps the injected CO_2 at a supercritical condition (Orr, 2009; Bachu et al, 2004). Also, there must be an effectively impermeable caprock that is not fractured in order to keep the CO_2 from leaking to the surface. The storage potential of each reservoir is determined using a suite of geophysical data. In addition to well logs, 2-D seismic reflection data help to determine the lateral continuity of formations surrounding Plant Gorgas. Prior to the study, wells that penetrated the formations below Mississippian units in this part of the basin were sparse, and available seismic data are sparse and/or of poor-quality. Past studies have mediocre well-seismic ties because of poor quality seismic data and a lack of check-shot surveys.

2.0 GEOLOGIC SETTING

2.1 Tectonics

The Black Warrior Basin developed during the Paleozoic construction of Pangaea as collisions occurred on the eastern and southern margins of the Laurentian landmass. The Ouachita Embayment underwent multiple stages of active rifting during the development of the Rheic and Iapetus Oceans as evidenced by the Mississippi Valley Graben and the Birmingham Graben systems (Thomas, 1988; Thomas and Whiting, 1994; Murphy et al., 2006; Groshong et al., 2010). The region continued as a passive margin for 200 million years with an extensive carbonate platform until the Ouachita terrane accretion event occurred in the Late Mississippian. Today, the Ouachita fold and thrust belt stretches from the Alabama Promontory through western Texas, but it has mostly eroded and is buried by Cenozoic sediments of the Gulf Coastal Plain in Alabama and Mississippi (Pashin and Gastaldo, 2009).

The Black Warrior Basin is a homocline that dips southwest beneath the Ouachita thrust front (Thomas and Whiting, 1994). The load from the Ouachita thrust belt created a depression in the adjacent crust, also known as a foredeep, causing a peripheral bulge to propagate in a northeasterly direction (Moores and Twiss, 1992; Watts, 1992; Ettensohn and Pashin, 1993; Turcotte and Schubert, 2002). Synorogenic sediments infilled the foredeep adjacent to the Ouachita thrust front. The clastic wedge extends northeast to the Nashville Dome. On the eastern margin of Laurentia, Appalachian Mountain building events span from Ordovician through the Pennsylvanian time, ending with the Alleghanian orogen confining the Black

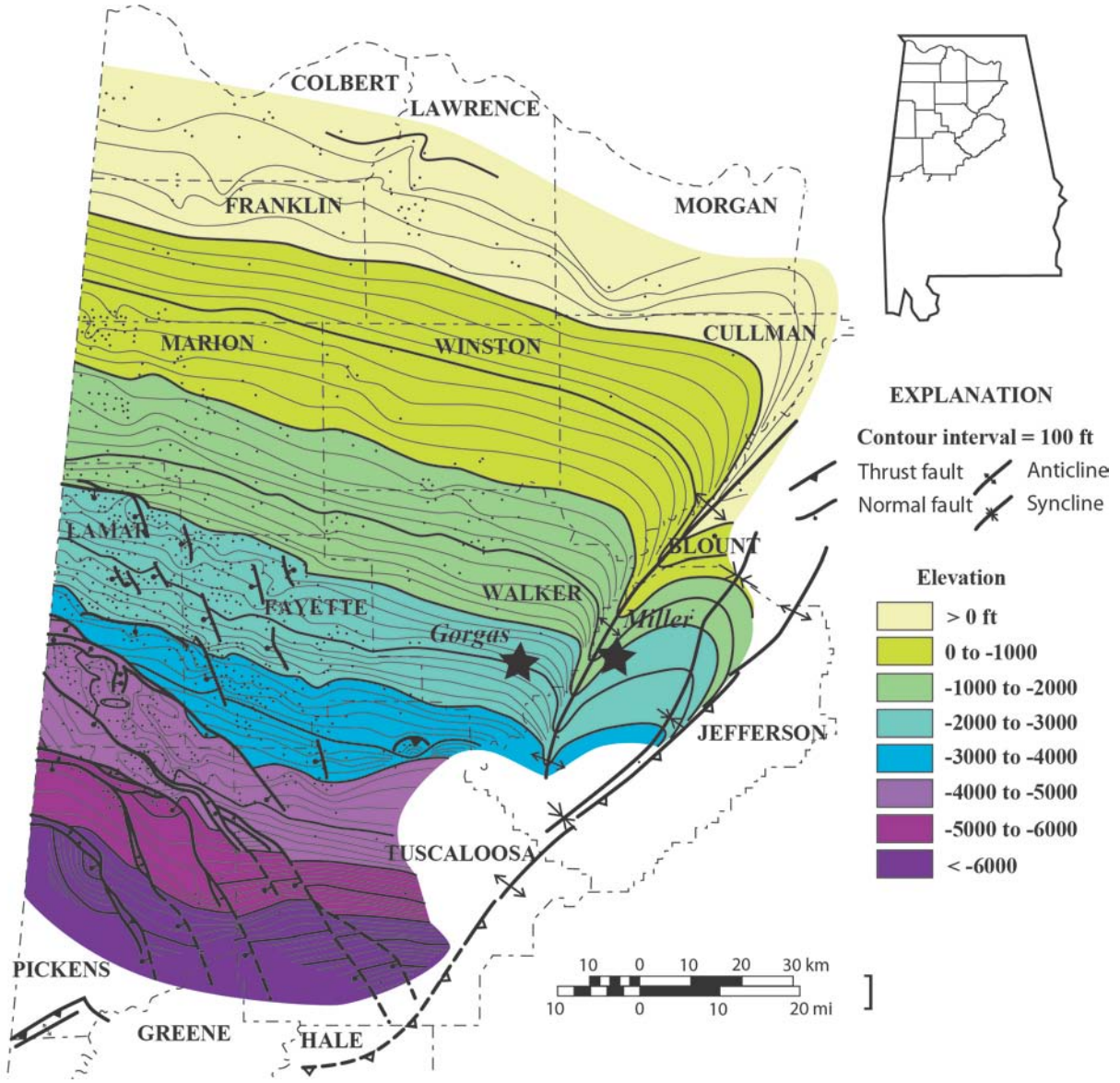

Figure 2: Regional dip of the Tuscumbia Limestone within the Black Warrior Basin (modified from Pashin, 1993). Dashed lines mark county boundaries. Plant Gorgas and Plant Miller are marked by black stars. Colors depict depth in the subsurface relative to mean sea level. The unit dips towards the Ouachita thrust front to the southwest and the majority of the normal faults dip to the southwest with the exception of the graben forming antithetic faults. The majority of the faults sole into the Pottsville detachment and have been interpreted based on shallow coal bed methane wells. Basement normal faults in the basin form horst and graben structures and are primarily oriented from northwest to southeast along regional strike of the Ouachita thrust belt. The Gorgas #1 well is in Walker County, Alabama; six miles west of the Sequatchie Anticline, the site of the western most thrust on the eastern edge of the basin.

Warrior Basin to its present location. This created two primary sediment sources for the Black Warrior Basin; the Ouachita orogen from the southwest and the Alleghanian orogen from the east and southeast (Thomas, 2004; Thomas, 2006; Pashin and Gastaldo, 2009; Groshong et al, 2010). The collision of Laurentia and Gondwana concluded Alleghanian-Ouachita orogenesis, which lead to an era of erosion and subsidence in Early Pennsylvanian time (Miall, 2008).

The majority of faults in the basin predominately trend northwest-southeast, parallel to the Ouachita thrust front. Few normal faults follow the trend of the Appalachians. The eastern part of the basin is dominated by normal faults that maintain a planar 60° - 70° dip until terminating at a thin-skinned detachment in the lower Pennsylvanian Pottsville formation. To the west, some faults extend to a deeper thin-skinned detachment near the base of the Knox Group carbonates and are typically interpreted as listric characterized by wide hanging-wall rollover structures (Groshong et al., 2010)

2.2 Stratigraphy

The regional stratigraphy of the area is constrained using well log data and existing seismic reflection profiles (Pearce, 2002; Maher, 2002; Gates, 2006; Robinson et al, 2009; Groshong et al., 2010). The basin is predominately composed of clastic and carbonate units that reflect the tectonic and paleoceanographic changes within the basin (Pashin and Gastaldo, 2009). Stacked saline aquifers make up a large portion of the stratigraphic framework and extend throughout the Black Warrior Basin making them ideal candidates for sequestration.

The oldest stratigraphic unit found in the characterization well (Figure 3) is the Middle to Late Cambrian Conasauga Formation. This formation has fine-grained clastic and carbonate rocks

associated with late-synrift extension that interrupted the growth of a passive margin carbonate platform (Thomas, 1989; Thomas, 2007). The fine-grained clastic rocks of the Conasauga and underlying Rome Formation act as the main detachment surface for Alleghanian thrusting (Thomas and Bayona, 2002). The overlying Cambrian–Ordovician Knox Group is composed of limestone and dolostone deposited on the passive margin carbonate shelf in a restricted hyper-saline environment, and represents a time of maximum transgression. Regionally, the unit is 914 - 1524 m (3000 - 5000 ft) thick (Osborne and Raymond, 1992). The Middle Ordovician Stones River Group and Upper Ordovician Sequatchie Formation represent varying tidal environments on a carbonate shelf. The Stones River Group consists predominately of fine-grained argillaceous limestone with fossil horizons and bentonitic shales. A typical regional thickness for the Stones River Group ranges from 243.8 m (800 ft) to more than 304.8 m (1000 ft; Chowns and McKinney, 1980). The Sequatchie Formation has a highly variable lithology throughout northern Alabama consisting of interbedded shale and limestone. It is the most widespread Upper Ordovician unit in the state, typically ranging from its maximum of 167.5 m (550 ft) in the Sequatchie Anticline to 15 m (50 ft) to the south of the anticline (Drahovzal and Neathery, 1985; Ferrill, 1989). The Silurian Red Mountain Formation and the Devonian Chattanooga Shale are synorogenic deposits shed from the east during the Taconic and Acadian orogenic events. The Red Mountain Formation is a heterogeneous succession of mudstone, sandstone, and limestone (Thomas, 2007). The base of the Red Mountain Formation is typically identified by oolitic ironstone. The Chattanooga Shale is a black fissile shale that ranges from 0 - 27 m (0 – 90 ft) thick and is widespread throughout the Black Warrior Basin (Pawlewicz and Hatch, 2007; Pashin, 2008; Pashin et al., 2010). The Lower Mississippian Fort Payne Chert and Tuscumbia Limestone are indicative of the persisting passive margin carbonate shelf along the western and

southern edges of the Alabama Promontory (Figure 1). The Fort Payne Chert is composed of siliceous micrite and bluish-gray nodular chert that has a gradational contact with the overlying Tuscumbia Limestone. Together these units have a maximum thickness of more than 137 m (450 ft) in the northeast section of the basin that thins southwestward to less than 7.6 m (25 ft; Pashin, 1993). Late Mississippian arc-continent collisions along the southeastern edge of the continent heralded in a time of synorogenic clastic wedge progradation and interfingering between siliciclastic and carbonate depositional systems. A disconformity at the base of the Pride Mountain Formation marks the beginning of Ouachita orogenesis along the southwestern margin of the Alabama Promontory (Thomas, 1989; Thomas, 2007; Pashin and Gastaldo, 2009). The Pride Mountain Formation, a heterogeneous unit comprised of shale, limestone, and quartz arenite sandstone, was deposited in a low-stand wedge on the northern shelf of the Black Warrior Basin (DiGiovanni, 1984; Cleaves and Stapor, 1992). The Hartselle Sandstone forms a belt trending northwest to southeast and is up to 128 km (80 miles) wide and no more than 49 m (160 ft) thick in the basin (Thomas and Mack, 1982; Cleaves and Stapor, 1992). Regionally, it is a well-sorted, fine-grained, cross-laminated quartz arenite, which represents a barrier strand-plain complex fed by long-shore drift carrying reworked sands deposited on the southwest side of the Nashville Dome (Thomas, 1989; Pashin, 1993). Rising sea levels caused transition from a transgressive to a highstand systems tract in the Late Mississippian, and led to the deposition of the Bangor Limestone, a medium to dark grayish-tan limestone deposited on a carbonate platform. The Bangor Limestone thins southwestward from a widespread uniform thickness of 107 – 137 m (350 – 450 ft) to less than 30 m (100 ft) in southwestern Alabama where it grades into the time equivalent Floyd Shale, a deep water, organic rich marine shale deposited in the deeper parts of the basin (not present in the study area). Progradation of the carbonate shelf

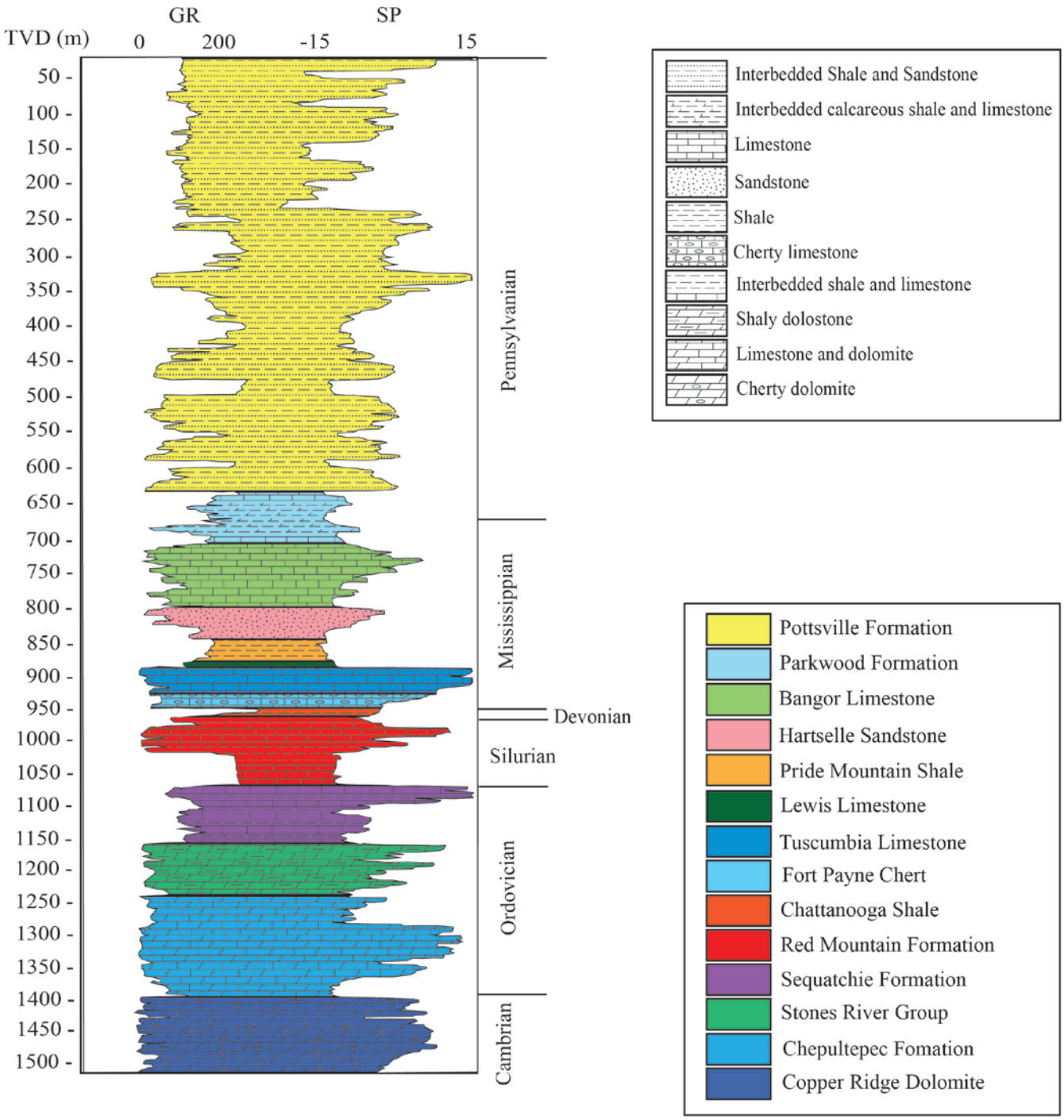

Figure 3: A stratigraphic section for the Gorgas #1 well showing formation thickness, lithology, spontaneous potential (SP) and gamma ray (GR) content.

established a southwest dipping clinoformal slope that was a dynamic foundation to the thickness and facies distribution in the overlying Parkwood Formation (Pashin, 1993; Pashin, 1994). The transition from marine transgression and carbonate sedimentation to siliciclastic-dominated successions in the Middle Parkwood indicates basin migration from the southern trade-wind belt into the equatorial rainy belt at the Mississippian-Pennsylvanian boundary (Thomas et al., 1991; Scotese and Golonkas, 1992; Pashin and Gastaldo, 2009). At this time, the Alleghanian orogeny began supplying a large amount of coarse-grained sediment into the Black Warrior Basin (Pashin, 1994; Pashin and Gastaldo, 2009). The Pottsville Formation is composed of multiple cyclothems, defined by marine-nonmarine depositional cycles resulting in the layering of sandstones, shales, and coals. This sequence of rock type is ideal for storing injected CO_2 because the thick sandstone units are capped by impermeable shales and coals. The Pottsville Formation averages a thickness of 762 m (2500 ft) and is the youngest preserved strata in the basin. Two thick sandstones, the Fayette and the Boyles, are characteristic units of the Pottsville Formation. Both units are composed of quartz arenite and were deposited in a beach-barrier island to tide-dominated shelf environment (Thomas, 1989; Pashin and Gastaldo, 2009).

3.0 CARBON SEQUESTRATION

In recent years, research points to increased amount of greenhouse gas emissions, including CO_2, as the cause for global temperature rise (Hazeldine, 2009). Sequestering CO_2 into deep geologic units has been in practice since the 1970's as a form of enhanced oil recovery and has been used as a form of mitigation since the mid-1990's at sites such as Sleipner in the North Sea, the In Salah site in Algeria, and the Weyburn site in Alberta, Canada (Zhaowen et al., 2006). Emissions are mitigated by capturing CO_2 from coal-fired power plants then sequestering it into deep geologic units such as depleted oil and gas fields, coal seams, salt caverns, or saline reservoirs (Orr, 2009). When CO_2 is injected underground, the pressure in the subsurface causes the volume of the gas to decrease, maximizing storage volume. Additionally, CO_2 reaches a supercritical state at a temperature and pressure of 31.1^{o} C and 72.9 atm (7.39 MPa), respectively. For CO_2 to remain as a supercritical fluid, it must be injected below a depth of 755.9 m (2480 feet; Orr, 2009). This allows CO_2 to disperse into the pore spaces like a gas while approaching liquid density

4.0 DATA AND METHODS

Multiple investigations were completed to characterize the geologic structures and stratigraphy in the subsurface beneath Gorgas Power Generation Plant. A stratigraphic test well was drilled at the plant with a total depth of 1498 m (4915 ft), and a suite of geophysical wireline logs was collected. In addition, a ZVSP and 10 miles of 2-D surface seismic reflection data were acquired and used for a geophysical and stratigraphic characterization around Plant Gorgas.

4.1 2-D Seismic Reflection Data

2-D seismic reflection data were collected along two 8.05 km (5 mile) lines. The closest line (Line 201) is 1.28 km (0.795 miles) north of the well site (Figure 4). Line 101 has a north-south orientation and follows County Road 6. Line 201 is oriented northwest-southeast on State Highway 269, perpendicular to the axial trace of the Sequatchie Anticline. Seismic data were collected using three Hemi-44 Vibroseis trucks with a 19,958 kg (44,000 lb) peak force. The trucks performed four, 6 - 100 Hz, 4 -12 second sweeps at each location with a record length of 5 seconds and a sample rate of 2 ms. The distance between shots was 36.58 m (120 ft), and the receiver interval was 3.05 m (10 ft). The receivers had a digital group formed every 12.9 m (40 ft). The maximum offset attained between source and receiver was 8047.72 m (26400 ft). A complete list of the acquisition parameters is given in Table 1.

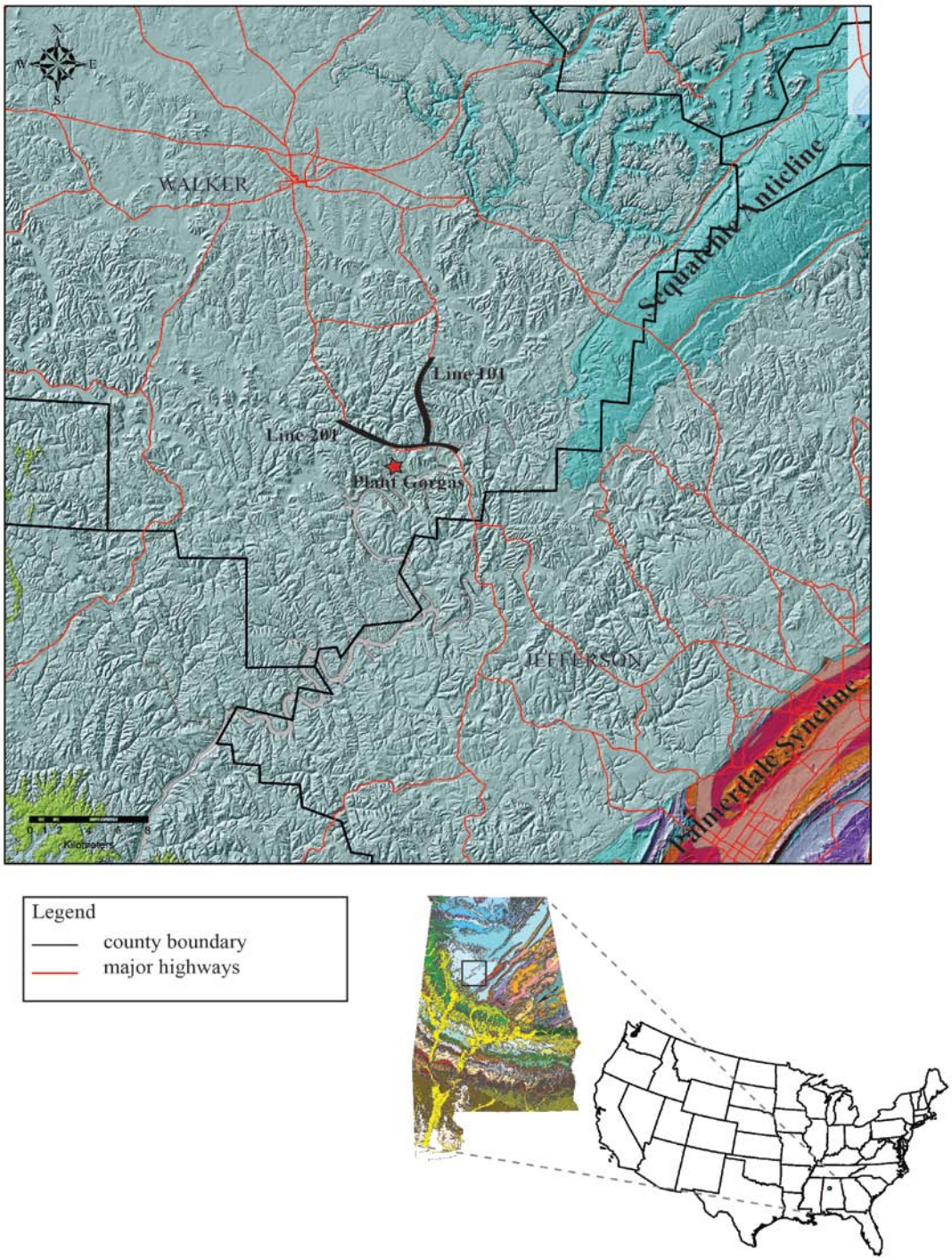

Figure 4: Geologic map showing the location of Plant Gorgas characterization site and acquisition lines for the 2D seismic reflection survey in Walker County, Alabama. Plant Gorgas is on the eastern side of the Black Warrior Basin in close proximity to the Sequatchie Anticline. The Pennsylvanian Pottsville Formation is the only unit at the surface (grayish blue). In our study area, two five mile long lines were collected. A broadly north-south strike line (Line 101) was acquired along County Road 6. This line ends at Highway 78. A roughly east-west dip line (Line 201) was acquired along State Highway 269. Line 201 is 1.28 km (0.795 miles) north of the test well drilled at Plant Gorgas.

Acquisition	
Source	
Source (Vibroseis)	X3 Hemi-44, 20411.65 kg (45,000 lb) trucks
Source Interval	36.5 m (120 ft)
Shot Density / sq mile	44 Vps
Receivers	
Receiver Interval	3.048 m (10 ft)
ITO Interval	36.5 m (120 ft)
DGF Interval	12 m (40 ft)
PR Density / mile	528 single sensors
DGF Density /sq mile	132 Group Formed channels
Design Patch	
Total Channels/Line	8 km (5 mile) lines all live
Design - DGF/Line	1 x All live Digital Group Formed channels
Recording Statistics	
Total Live Channels	All live point receivers
Effort	4 - 12 sec sweep per location
Sweep Type	6 - 100 Hz Phase Rotated Sweep
Record Length	5 seconds
Sample Rate	2 ms
Subsurface Statistics	
Bin Size	6 m (20 ft)
Bin Density	264 per mile
Nominal Fold	110 post DGF
Minimum Offset	6 m (20 ft)
Maximum Offset	8047 m (26,400 ft)

Table 1: Acquisition parameters for seismic reflection data. ITO = Intelligent Take-Out Interval, DGF = Digital Grouped Formation, PR = Point-Receiver

The survey used the Schlumberger Q-land system. This allows for the option of using single sensors rather than relying on the signal from a group of sensors. If there is noise on a single sensor, the Q-land system allows for that signal to be isolated rather than corrupting the receiver group. This method is useful for detailed static corrections where the topography is rugged. Static corrections were referenced to a seismic reference datum (SRD) at 244.844 m

(800 ft) above mean sea level using a 4572 m/s (15000 ft/s) replacement velocity. Data processing was completed by Schlumberger (Table 2) to produce pre- and post-stack time migrated seismic sections.

The seismic data are zero-phase. Seismic data collected using a Vibroseis source is also known as a correlogram. This is derived after the sweep is cross-correlated with the data that has been recorded on the accelerometers. The cross-correlation process creates a peak at each reflection event (Stark, 2008). Interpretations of the seismic reflection profile were completed after the synthetic seismogram was generated to ensure accurate ties between depths of units interpreted from the geophysical logs and reflectors on the seismic reflection profile. Horizons were picked on peaks that corresponded with unit contacts. In some instances a trough was picked because the formation was either too thin to produce a top and bottom reflection or due to effects from tuning, which will be addressed in the results section. A topographic high in the center of Line 101 (Figure 5) is coincident with increased noise levels. This area is adjacent to vertical faces associated with coal mine high-walls adjacent to the road; this may have resulted in ray paths not accounted for in the preliminary 2-D seismic reflection processing. Two zones along Line 201 (Figure 6) at common mid-point (CMP) 237 and CMP 781 are treated with caution because bridges along the road required a gap in the receiver distribution. Anomalous dips may result from locally low-fold CMPs that prelude good velocity picks and hence corrections of Normal Move Out. More detailed processing, beyond the scope of this project, will focus on improved imaging in these areas.

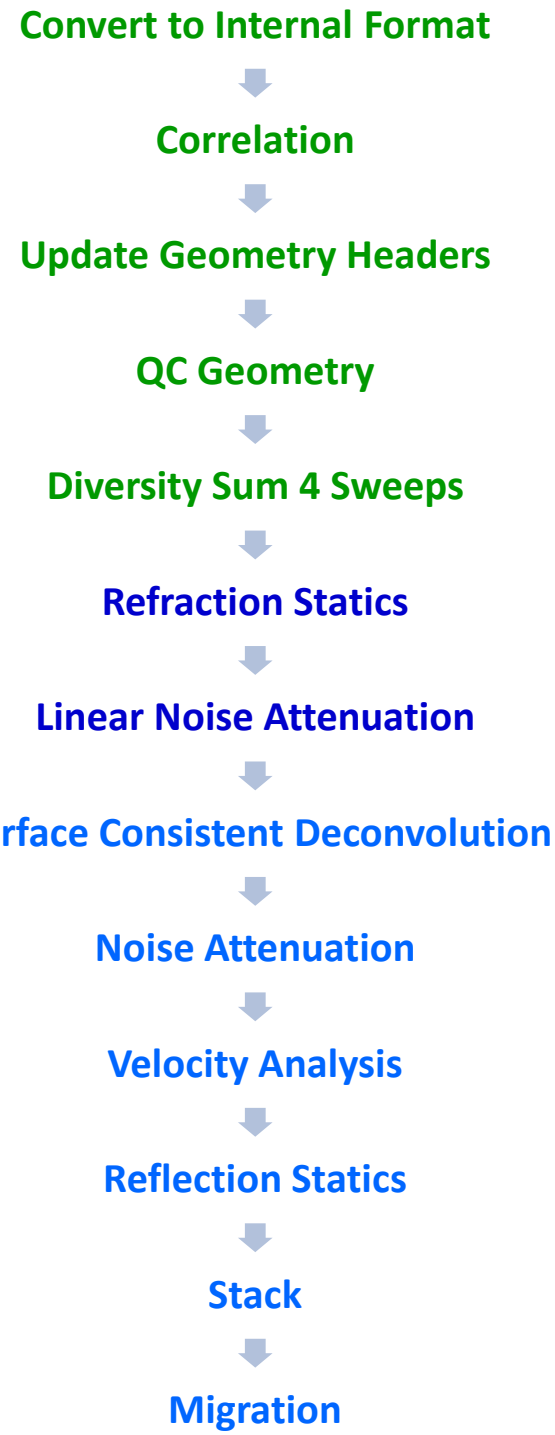

Table 2: Processing flow of post-stack time migrated 2-D seismic reflection profiles for Line 101 and line 201. QC = Quality control.

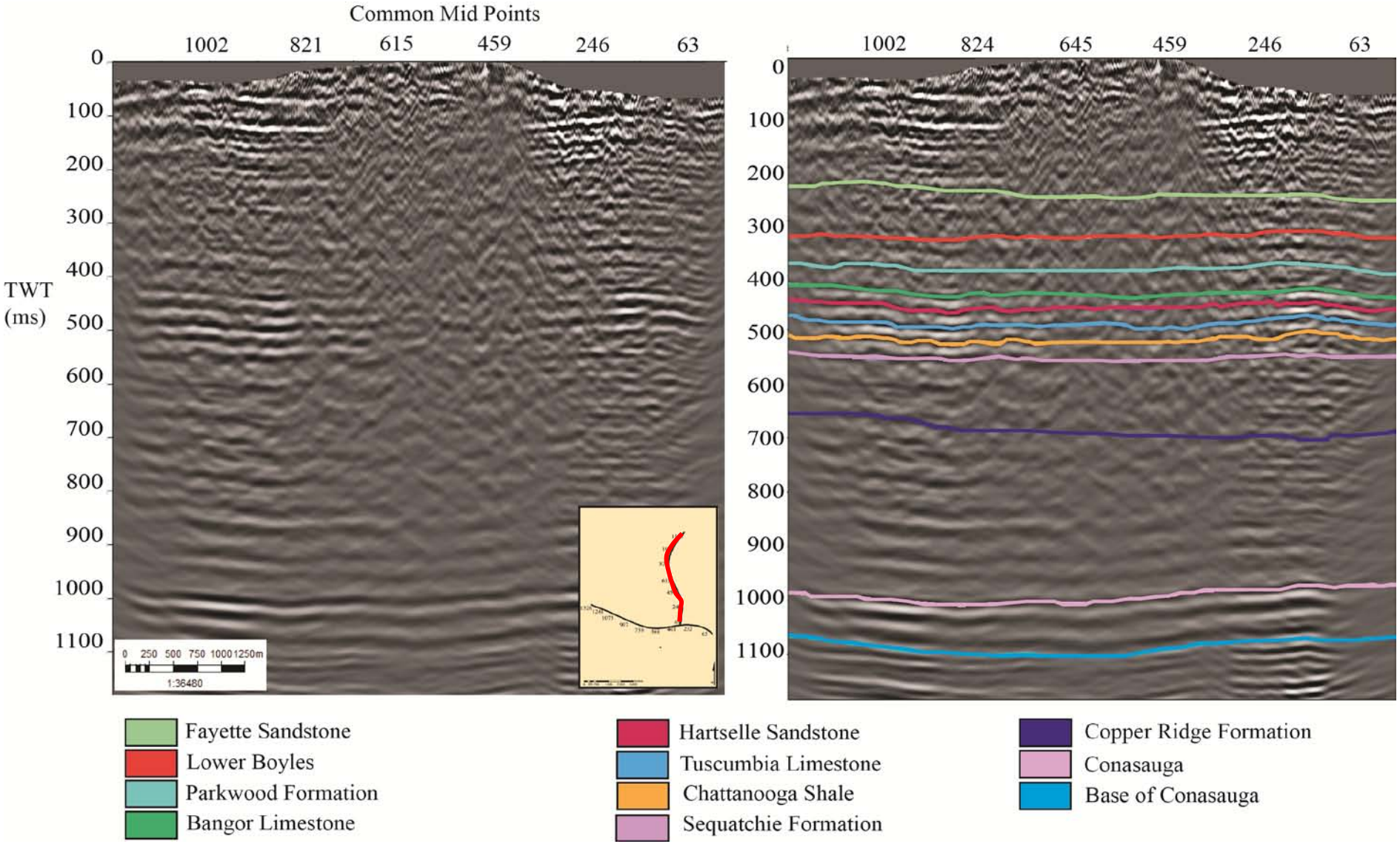

Figure 5: Pre-stack time migrated 2-D seismic reflection profile for Line 101 prior to depth conversion. On the right side is Line 101 with formation tops interpreted. The profile is broadly oriented north to south. The CMP spacing 6 m (20 ft). The vertical scale is in milliseconds (ms). Target reservoirs lie below the Lower Boyles Sandstone (~300 ms). The line passes over a topographic high between CMPs 896 and 288.

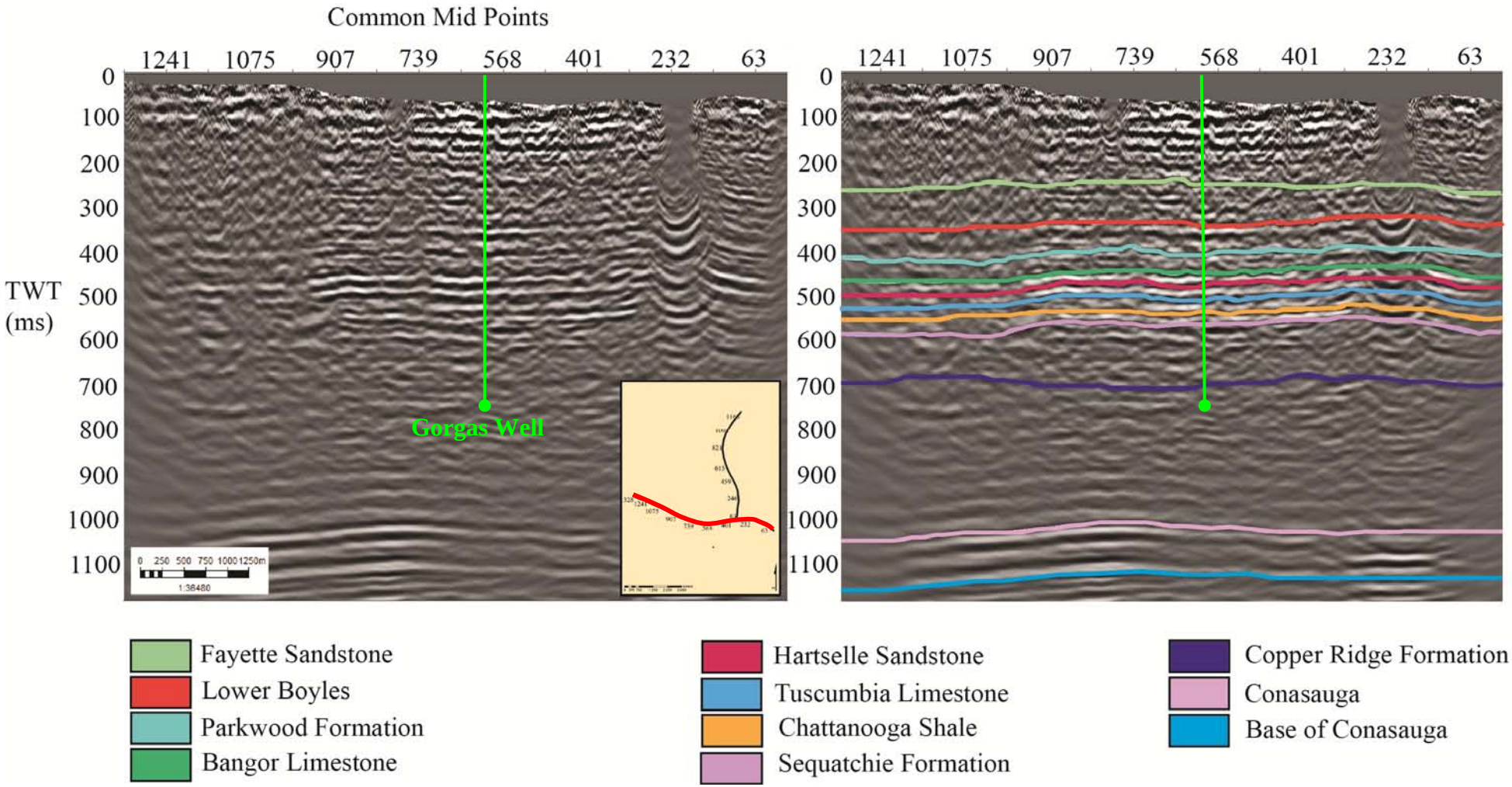

Figure 6: Pre-stack time migrated 2-D seismic reflection profile of Line 201 prior to depth conversion. On the right side is Line 201 with formation tops interpreted. The profile is oriented west to east. The CMP spacing is 6 m (20 ft). The vertical scale is in milliseconds (ms). The well reached a total depth in the Copper Ridge Formation at approximately 4915 ft (700 ms). Reflector disturbance under CMP 232 is due to the presence of a bridge where there was a gap in accelerometer deployment.

4.2 Check-Shot Data

Check-shots supply the most accurate time-to-depth conversion because they take a direct measurement of time for a signal at the surface to reach a receiver at a given depth in the borehole. For the check-shots, the Vibroseis source had a horizontal offset of 49 m (162 ft) to the northwest of the well, with a vertical offset of 4.18 m (13.74 ft) below the Kelly Bushing (KB; Figure 7). Measurements were taken downhole at 15 m (50 ft) intervals between 30 and 1478 m (100 - 4850 ft) depth. The Check-Shot report (Appendix Ia) provides depths from the KB and the seismic reference datum (SRD; 244 m (800 ft) above sea level), acoustic average velocity, root-mean-square (RMS) velocity, interval velocities calculated between each measurement level, and vertical one-way transit time corrected for source offset with static corrections applied. Correcting for a vertical well is necessary because there was a small offset between the Vibroseis source and the well head. This was achieved by first applying a static correction to the measured depth (MD) and then finding the oblique distance between the source and down-hole receiver using MD from KB and the horizontal offset distance. The angle of the incoming ray-path was calculated, and a verticalized one-way transit time was derived using the offset angle and one-way times provided in the report. A separate velocity report (Appendix Ib) includes average, interval, and RMS velocities using down-hole sonic log data to interpolate between check-shot levels. A recalculation was made using the method of Linari (2004), to ensure accuracy of travel times corrected to a vertical well. Velocities were recalculated using the change in depth over the change in time ($\Delta z/ \Delta t$) for accuracy of the velocity model. These data are essential in the depth conversion of the seismic reflection data that was collected 1.28

km (0.795 miles) to the north. All travel times were calculated in relation to the seismic reference datum.

4.3 Zero-Offset Vertical Seismic Profile

The zero-offset vertical seismic profile (VSP) was acquired simultaneously with the check-shot survey. Acquisition was carried out using a Vibroseis truck source with 21,409.55 kg (47200 lbs) peak force and a 12 second 8 - 96 Hz sweep (Table 3). The receiver array comprised 4 receiver levels separated by 15.2 m (50ft). This was lowered to the base of the hole and progressively moved up the hole as measurements were taken. Basic data processing included stacking the data, automatic gain control, applying a band-pass filter of 5 – 100 Hz, temporal amplitude recovery, spatial amplitude normalization RMS, applying a median velocity filter on the up-going and down-going wavefields, then waveshape deconvolution. Creation of a corridor stack was accomplished using a narrow stack window of the zero phase deconvolved up-going wave-field, ensuring a multiple free 1-D response to compare side by side with the seismic reflection data. The VSP corridor stacks have a window length of 0.100 seconds and were filtered with a band-pass filter using frequencies ranging from 8 - 40, 50, 60, and 80 Hz in order to find the best match with the frequency content of the seismic reflection data (Figure 8; Campbell et al., 2005). The best frequency match with the seismic reflection data was the 8 – 40 Hz corridor stack. Due to the shorter path length of the seismic wave in a VSP in comparison to conventional 2-D reflection seismic data, the higher frequencies provide better resolution. The interpreter can use this to evaluate stratigraphic variations and the acoustic impedance responses of target formations in greater detail. The higher frequency stacks are valuable for imaging

thinner formations such as the Chattanooga Shale, which is below the resolution of the seismic reflection data.

Zero – Offset VSP	
Tool	VSI-4
Geophone	GAC-D
Sample Rate	2 ms
Receiver Range	1478.28–30.48 m (4850-100 ft)
Receiver Interval	15.24 m (50 ft)
Source Type	Vibroseis
Source Offset	49.37 m (162 ft)
Source Azimuth	345 degrees
Elevation	114.6 m (376.10 ft)

Table 3: Zero-Offset vertical seismic profile acquisition parameters, VSI = Virtual Seismic Imager; GAC-D = Geophone Accelerometer with Dampening.

4.4 Wireline Logging Data

The well reached a total depth of 1498 m (4915 ft) in the Upper Cambrian Copper Ridge Formation. All well logs and mud logs (Appendix II) were used during interpretation. The gamma ray log readings were used to determine lithologic boundaries and heterogeneity within units. The sonic and density logs were used to create a synthetic seismogram. The resistivity curve values were used to create a pseudo-sonic log in areas where sonic readings were affected by borehole breakout (rugosity along the sides of the borehole). Where the neutron and density porosity logs crossed over each other, they indicated porosity and gas effect.

The logging tools that made contact with the sides of the borehole are of poor quality between 840 m (2758 ft) and 880 m (2887 ft) due to a major washout in the Pride Mountain

Formation. In this interval the sonic and density logs required editing before being used to generate a synthetic seismogram in order to correct the extraneous values caused by poor coupling of the wireline tool with the borehole. The following editing techniques were applied: smoothing (triangular filter), despiking, and clipping extreme values. In addition, 3 m (10 ft) of the log between 870 to 874 m (2856 to 2867 ft) is missing. A sonic log was derived from resistivity for the 3 m (10 ft) missing section using a "scale function" (Kim, 1964) in IHS Kingdom Suite. This is a predictive method that creates a synthetic sonic log using a relationship derived between sonic and resistivity in an intact portion of the borehole (AF90; See Appendix III; Rudman et al, 1975; Smith, 2007). This method is preferred over the more traditional Faust's formula (Faust, 1953) in cases where both the sonic and resistivity logs exist for a borehole, but the sonic log has been affected by washout zones.

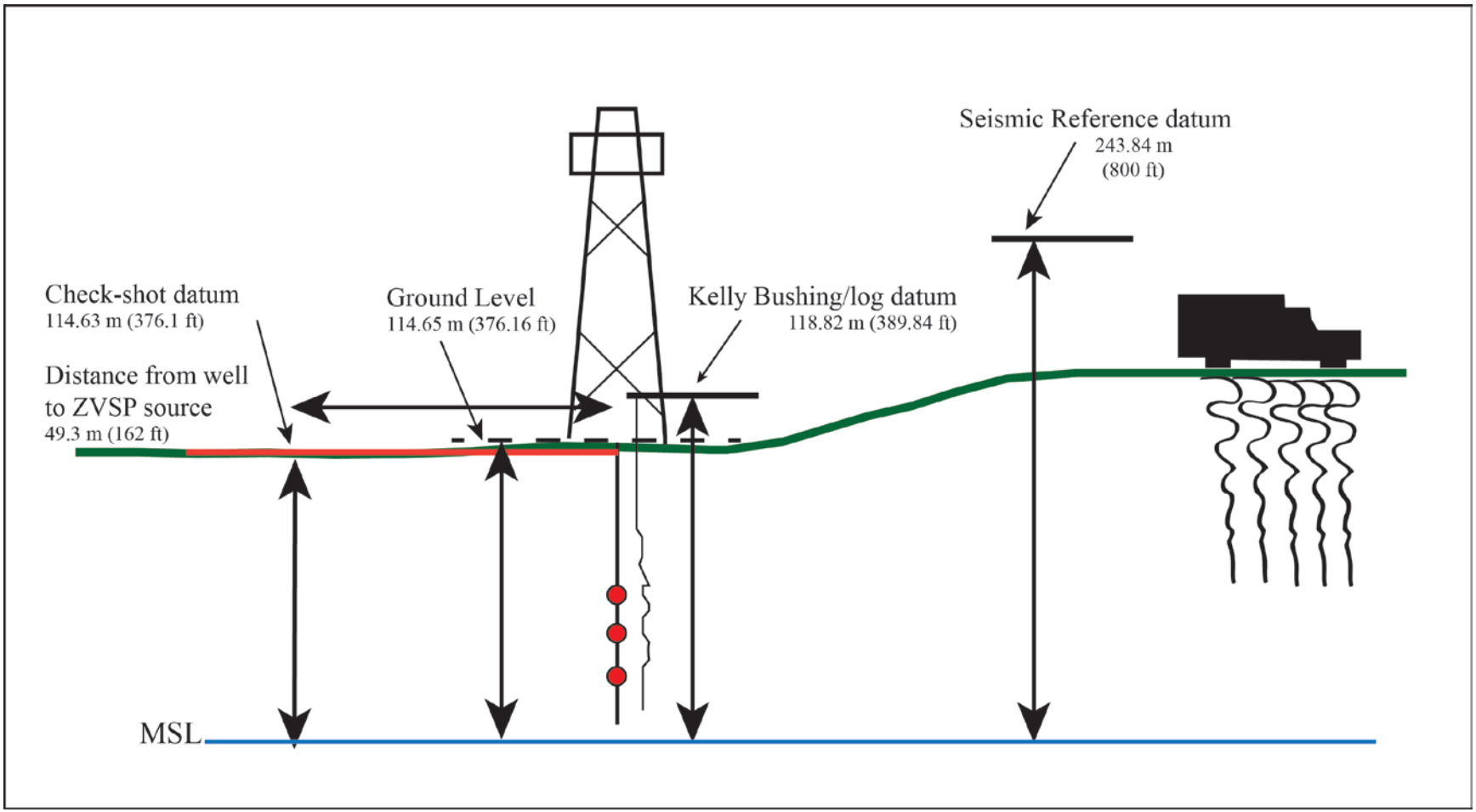

Figure 7: Datum elevations for the 2-Dseismic reflection data, check shot data, and geophysical log data. During analysis the check-shot data were corrected to the SRD to ensure proper alignment of key reflectors. The check-shot datum is slightly lower than the ground level under the Kelly Bushing because of an offset of 49.3 m (162 ft) of the Vibroseis source.

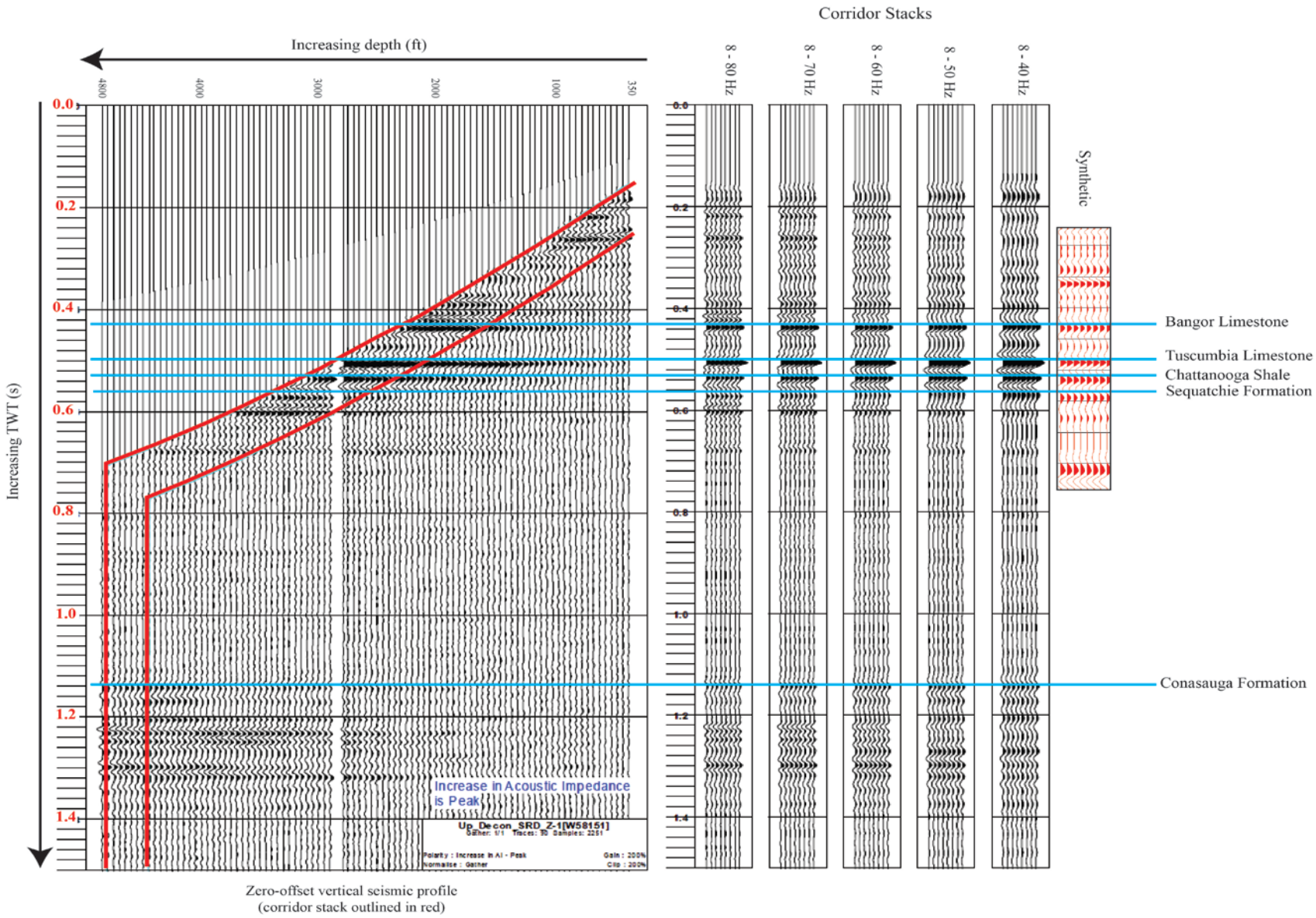

Figure 8: ZVSP after initial processing. The panel outlined in red is the section of the data used for the corridor stack. Corridor stacks (right) are displayed for a range of frequency contents. The synthetic seismogram (red) generated from the well data is to the right of the corridor stacks. The synthetic shows the depth interval for the well compared to the deepest Conasauga Formation.

4.5 Synthetic Seismogram

A synthetic seismogram is a simulated seismic section computed from well data, which correlates the information gained down-hole with the seismic reflection data. Generating a synthetic creates a tie between the time and depth domains (Box et al., 2004). The check-shot survey was used to calibrate the sonic data. Due to a difference in sampling interval and frequency range, down-hole logs sample the stratigraphy at a much finer scale than a seismic wavelet, so creating a time - depth relationship from the sonic velocities will result in differences between the synthetic and seismic trace (Liner, 2004). Calibration addresses this difference; it involves comparing transit times between defined intervals from the check-shot and sonic log to ensure the accuracy of a time – depth relationship.

The reflection coefficient was calculated using the edited sonic and density logs. A zero-phase wavelet was extracted from the 2-D seismic reflection data and convolved with the reflection coefficient in Petrel to create the synthetic seismogram (Figure 9). The reflection coefficient was convolved with the extracted wavelet. The resulting synthetic seismogram compares very well with the zero-offset 8 – 40 Hz ZVSP corridor stack and 2-D seismic reflection profile extracted at CMP 580 (Figure 9). All key reflectors in the 2-D seismic reflection data were interpreted based on matching the seismic character of the synthetic seismogram and the 8 – 40 Hz ZVSP corridor stack. As sonic logs and vertical seismic profiles are sparse in this part of the Black Warrior basin, this survey is essential in providing a well-seismic correlation that represents this region of the basin.

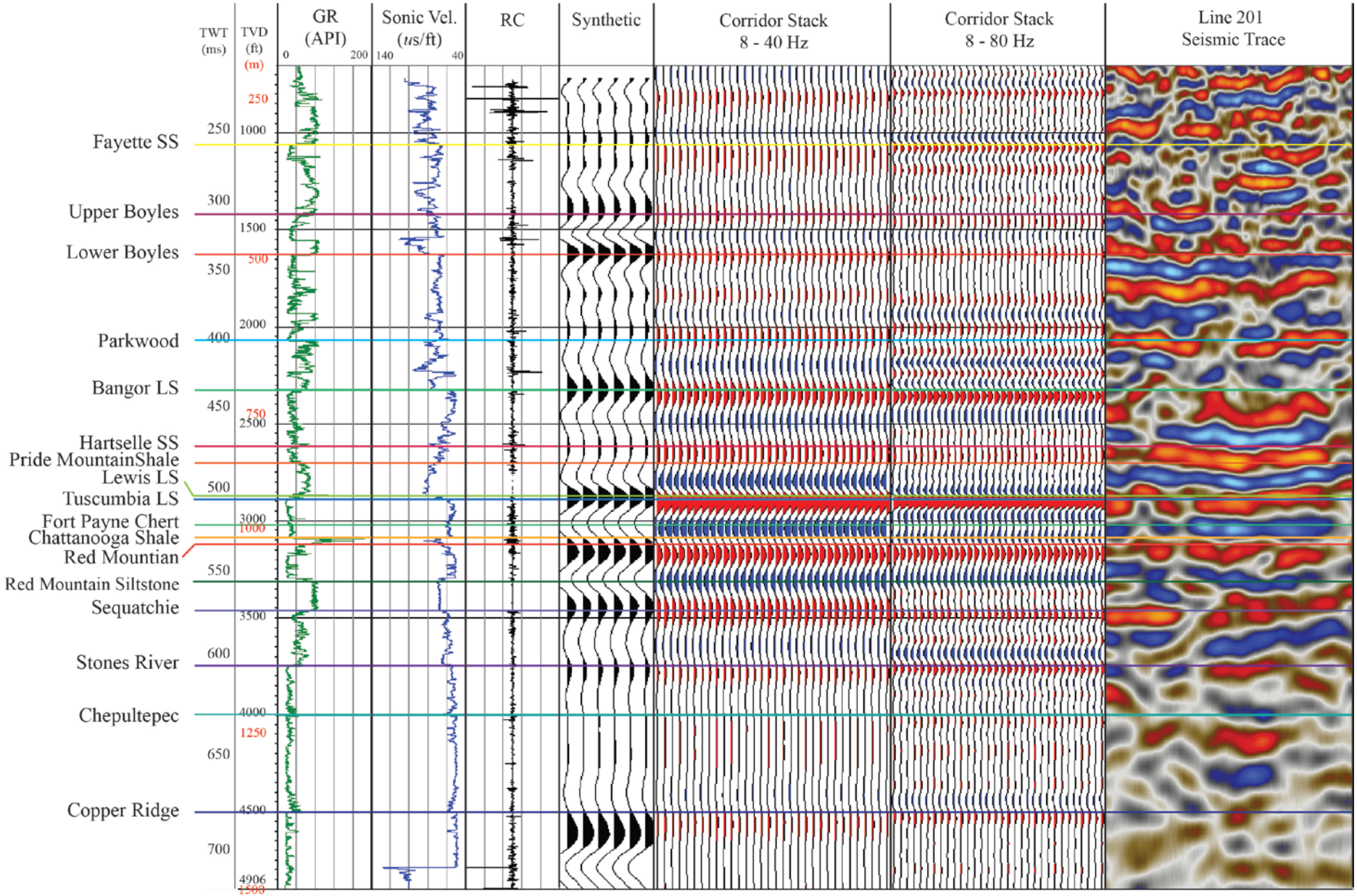
TWT (ms)
TVD (ft) (m)
GR (API)
0
200
Sonic Vel. (us/ft)
140
40
RC
Synthetic
Corridor Stack 8 - 40 Hz
Corridor Stack 8 - 80 Hz
Line 201 Seismic Trace
Fayette SS
Upper Boyles
Lower Boyles
Parkwood
Bangor LS
Hartselle SS
Pride MountainShale
Lewis LS
Tuscumbia LS
Fort Payne Chert
Chattanooga Shale
Red Mountian
Red Mountain Siltstone
Sequatchie
Stones River
Chepultepec
Copper Ridge
250
1000
300
1500
500
350
2000
400
750
2500
450
3000
1000
500
550
3500
600
4000
1250
650
4500
700
4906
1500

Figure 9: Down-hole logging, synthetic seismograms, ZVSP, and seismic reflection data for the Gorgas #1 well. The scale is depth in units of feet (black), meters (red), and two way travel time (TWT). The gamma ray (GR) log (green) is a reference log useful in identifying shale units. The sonic log (blue) is especially useful in differentiating sandstones from limestone when the GR count is low. The reflection coefficient (RC; black) is convolved with a wavelet that has been extracted from the 2-D seismic reflection data to derive the synthetic seismogram (black). The synthetic correlates very well with the corridor stack (red = peak; blue = trough). Two corridor stacks are shown: (left) filtered with an 8-40 Hz Butterworth wavelet, which has a closer frequency to the surface seismic data (Table 5), making it a good tool for the well seismic tie; (right) filtered with an 8 – 80 Hz, which allows the interpreter to resolve more detail concerning the thickness variation of units and heterogeneity below the resolution of the surface 2-D seismic reflection data. As an example, in the Parkwood Formation multiple peaks and troughs can easily be identified and correlated with the GR and sonic velocity to determine heterogeneity of the formation. Both the synthetic and the corridor stack tie well with the seismic trace (red = peaks; blue = troughs), which represents 50 traces surrounding CMP 580 on Line 201.

5.0 RESULTS

The time difference between the synthetic seismogram and the 2-D seismic reflection data is less than 10 milliseconds. The well-seismic tie shows that lithologic changes observed in wireline data correspond to key reflectors from stratigraphic units (Figure 9). Picks for unit tops in depth and time for the characterization well are shown in Table 4. Wireline readings begin at 218 m (716 ft) and stop at 1491 m (4894 ft). There are several transitions from clastic to carbonate rocks that create strong reflectors, but some units have thicknesses below the limit of vertical resolution (Table 5). Vertical resolution is the ability to resolve the top and bottom of an individual unit with reflectors on a seismic trace, and is equal to ¼ of the wavelength (Liner, 2004). Both vertical resolution limits and tuning effects can cause interference from thin beds. Tuning results when beds are approximately ¼ the seismic wavelength in thickness, and have strong enough acoustic properties that they interfere with the reflections from their upper and lower boundaries (Kallweit and Wood, 1982; Gochioco, 1991; Sheriff, 1999). This must be taken into account while doing any interpretations.

5.1 Wireline Log Interpretations

The Cambrian - Ordovician Knox Group is reached at a depth of 1221.3 m (4007 ft) at Plant Gorgas. The well passes through a 150.2 m (493 ft) section of Chepultepec Dolomite and

Surface	MD from SRD m (ft)	MD from KB m (ft)	TWT (ms)
Mary Lee Coal	100.84 (331)	-143 (469)	168.80
Jefferson Coal	-17.16 (252)	-252 (828)	225.13
Fayette Sandstone	-87.16 (322)	-322 (1058)	260.77
Upper Boyles	-196.16 (616)	-431 (1416)	311.39
Lower Boyles	-261.16 (827)	-496 (1627)	342.10
Parkwood	-396.16 (1271)	-631 (2071)	401.21
Bangor Limestone	-472.16 (1520)	-707 (2320)	434.31
Hartselle Sandstone	-562.16 (1815)	-797 (2615)	479.28
Pride Mountain	-589.16 (1902)	-824 (2702)	479.05
Lewis Limestone	-614.16 (2074)	-876 (2874)	504.19
Tuscumbia Limestone	-645.16 (2088)	-880 (2888)	506.46
Fort Payne Chert	-685.16 (2221)	-920 (3021)	521.98
Chattanooga Shale	-706.16 (2288)	-941 (3088)	529.26
Red Mountain	-717.16 (2324)	-952 (3124)	533.10
Sequatchie Formation	-822.16 (2667)	-1057 (3467)	572.64
Stones River Group	-907.16 (2946)	-1142 (3746)	603.79
Chapultepec	-986.16 (3207)	-1221 (4007)	630.70
Copper Ridge	-1137.16 (3700)	-1372 (4500)	678.89
Conasauga*	-2585.16 (8450)	-2820 (9250)	1144.32

*Only seen on seismic

Table 4: Two-way travel time (TWT; ms), measured depth (MD) from Kelly Bushing (KB), and Seismic Reference Datum (SRD) of formation tops at Plant Gorgas.

Velocity	5500 m/s (18045 ft/s)
Peak Frequency	30 Hz
Wavelength	183.3 m (601ft)
Vertical resolution	45.8 m (150 ft)

Table 5: Seismic reflection data from 500 ms was used to provide a representative velocity and peak frequency to calculation vertical resolution.

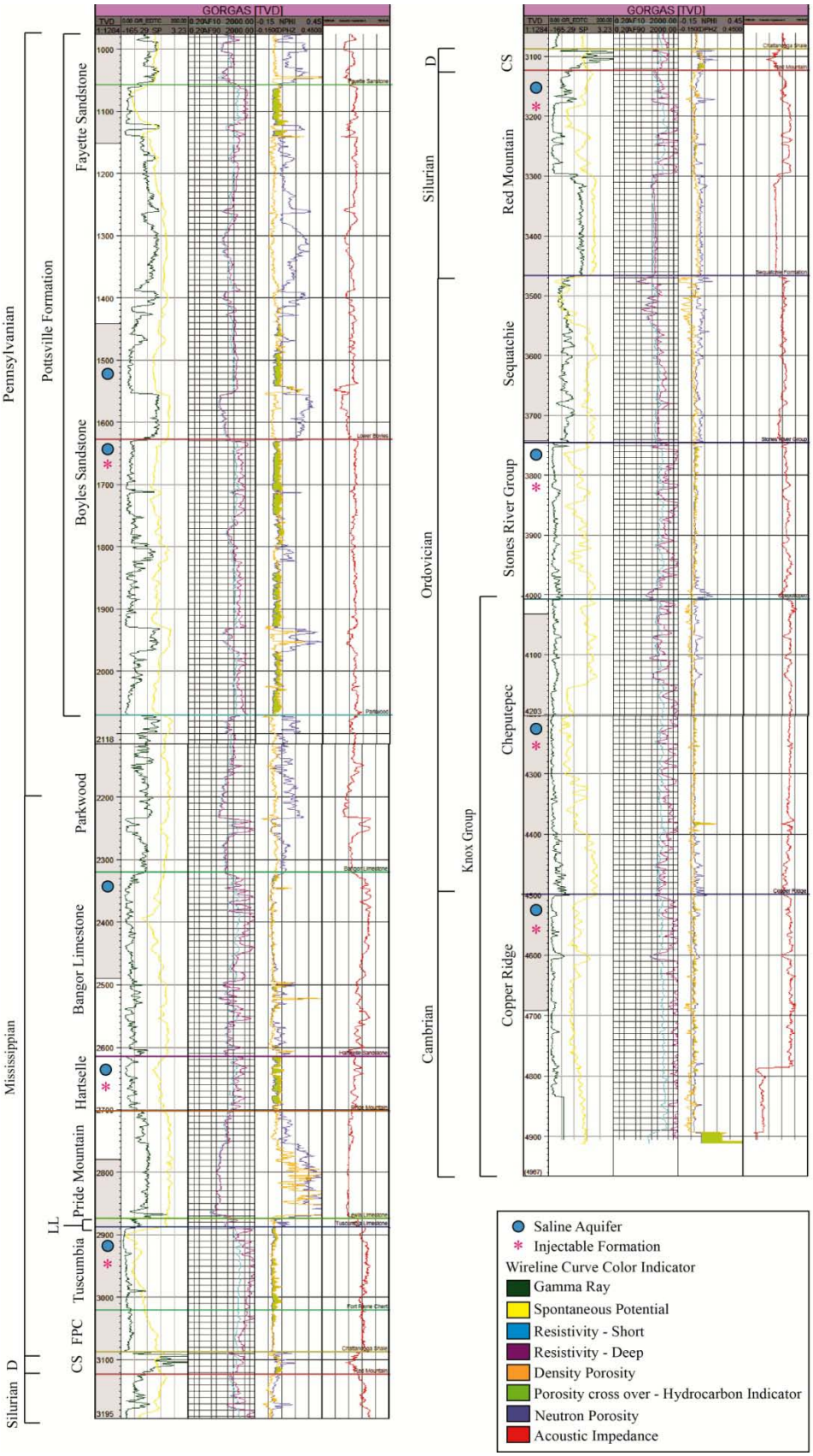

Figure 10: Detailed down-hole logs. Well tops are labeled as follows: LL = Lewis Limestone; D = Devonian; FPC = Fort Payne Chert; CS = Chattanooga Limestone; TVD = Total Vertical Depth (feet).

126.5 m (415 ft) of Copper Ridge Dolomite before reaching a total depth of 1498 m (4915 ft; Figure 10). Porosity in the Knox Group primarily results from secondary features such as vugs in algal structures, fractures, and subsurface solution features (Raymond, 1991; Osborne and Raymond, 1992). The Stones River Group is present from 1147 – 1226.5 m (3764 - 4007 ft) and has a thickness of 79.5 m (261 ft). The mud log shows that the upper Stones River Group contains 30.5 m (100 ft) of finely laminated black shale. The remaining 49 m (161 ft) of the lower Stones River Group is a dark gray limestone with no visible porosity. The Stones River Group was anticipated to be a good sequestration reservoir because it is a commercial gas reservoir in parts of the basin. However, the unit is thinner than expected and had a very low porosity (0.6 %) at the Gorgas site. Given that it is a gas producer elsewhere in the basin, it may need to be reevaluated for more accurate capacity values in the areas of the basin where it is being produced.

Overlying the Stones River Group, the Sequatchie Formation extends from 1057 - 1142 m (3467 - 3746 ft; Figure 10). The unit is 85 m (279 ft) thick beneath the Gorgas site. The mud log shows the Sequatchie Formation to be a medium to dark gray microcrystalline limestone with no visible porosity. It is interbedded with a calcareous dark gray to black shale throughout the unit. The Red Mountain Formation is a Silurian unit at a depth of 952 – 1056 m (3124 - 3467 ft) beneath Plant Gorgas. The unit is 104 m (343 ft) thick. The base of the Red Mountain Formation is identified by oolitic ironstone, which is recognized by elevated density measurements in the bulk density log. Mud logs show that the lower section of the Red Mountain Formation is a non-porous, greenish-gray siltstone that fines upwards into dark reddish-brown shale. The shale grades into a non-porous cream colored limestone in the upper 69 m (200 ft). The transition into the Devonian Chattanooga Shale is identified by an increase in

gamma ray log counts. The mud logs show that at this site the Chattanooga Shale is calcareous and interbedded with a gray fossiliferous limestone with pyrite in the laminations. Below Plant Gorgas, it is present from 941 – 952 m (3088 - 3124 ft; Figure 10).

The base of the Mississippian section is the Tuscumbia Limestone/Fort Payne Chert, present from 880 - 941 m (2888 – 3088 ft; Figure 10) beneath Plant Gorgas. The Tuscumbia Limestone/Fort Payne Chert has the best potential storage capacity volume with a thickness of 61 m (200 ft). It lies below the depth at which CO_2 becomes a supercritical fluid. The Tuscumbia Limestone had oil shows below Plant Gorgas, but is not a known reservoir throughout the basin due to poor sealing and a tendency to be fractured. It is likely that the Tuscumbia Limestone is only acting as a sealed reservoir at the Gorgas Site because it is highly cemented (Jack Pashin, 2012; personal communication). It would therefore be risky to inject CO_2 into the Tuscumbia Limestone because the areal extent of the cementation is unknown.

The Pride Mountain Formation is at a depth of 823.5 – 876 m (2702 – 2874 ft) and has a thickness of 52 m (172 ft; Figure 10). The mud log shows gray shale that has a gradational contact with the Hartselle Sandstone. The Hartselle is the fourth largest tar sand in North America (Wilson, 1987) and has potential for CO_2 storage and enhanced oil recovery (EOR). Below Plant Gorgas, the unit is at a depth of 797 – 823.5 m (2615 - 2702 ft) and is 26.5 m (87 ft) thick. From 797 - 803 m (87 - 107 ft), there are 6 m (20 ft) of thick asphaltic oil sands and 18 m (60 ft) of a light condensate indicated by core samples fluorescing blue to white under a black light. This type of fluorescence is indicative of an API gravity of greater that 40° (Jack Pashin, 2011; personal communication). Mud logs and crossovers between the density and neutron porosity show that the Hartselle Sandstone had approximately 24 m (80 ft) of hydrocarbons present (Figure 10). Regionally, this unit rarely exceeds 6 – 7.5 m (20 – 25 ft) of thick asphaltic

oil sands (Wilson, 1987; J. C. Pashin, 2011, personal communication). Core analysis is ongoing but average porosity logs indicate an average porosity of 5%. Oil saturation in the Hartselle throughout the basin averages 27%, but can range from 1- 60% with an average porosity of 13% in the saturated zone (Beavers and Boone, 1976). A simple guideline for CO_2 -EOR recommends that oil saturation be greater than 25% in the target reservoir (Bachu et al., 2004; Smith et al., 2009). Core analyses available on file at the Geological Survey of Alabama indicate that Mississippian quartz-arenite strandplain deposits typically have porosities of 6 - 19% and permeability ranging from 26 mD to as high as 663 mD. At the Gorgas site, porosities are very low due to a high percentage of cementation (J. C. Pashin, 2011, personal communication). Precise information concerning the Hartselle Formation at the Gorgas site will be available when core samples have been fully analyzed.

The Bangor Limestone is found beneath Plant Gorgas from 707 - 797 m (2320 – 2615 ft). The mud log shows that the upper 23 m (75 ft) is a microcrystalline, fossiliferous, and oolitic limestone with no visible porosity. The lower 67 m (220 ft) is interbedded with gray shale that lacks oolites and is less fossiliferous. There is a sharp contact between the Bangor Limestone and the underlying Hartselle Sandstone, most likely indicating a flooding surface at the end of a lowstand transgressive system tract (Cleaves and Stapor, 1992; Pashin, 1993). Below Plant Gorgas the Parkwood Formation is found at a depth of 631 - 706 m (2071 - 2320 ft) and is 75 m (249 ft) thick. The mud log shows a 60 ft section of microcrystalline limestone that grades into silty shale.

The Pennsylvanian Pottsville Formation is exposed at the surface and reaches a depth of 630 m (2071 ft). At Plant Gorgas it is composed of shales, six thin coal seams, and two

significant sandstone units: the Fayette sandstone and the upper and lower Boyles sandstone. The Fayette sandstone is reached at 322 m (1058 ft) and is 26 m (85 ft) thick, has silica cement, and showed no visible porosity. The upper Boyles sandstone is reached at a depth of 435.8 m (1431ft) and is 36.8 m (121 ft) thick. At the Gorgas site, the lower Boyles was 135.33 m (444 ft) thick but had little to no visible porosity due to silica cement. In addition, it is reached at a depth of 495.9 m (1627 ft) at Plant Gorgas, which is above the depth required for supercritical CO_2 conditions, making it an inadequate candidate for geologic sequestration.

5.2 Seismic Reflection Signatures

Many of the key reflectors have characteristic amplitudes on the 2-D seismic reflection, ZVSP, and synthetic data (Figure 9). Figure 9 includes reference logs, a synthetic seismogram, seismic traces, and two corridor stacks (one processed using a low frequency and one at a high frequency). The low frequency 40 Hz processed corridor stack is most representative of the overall surface 2-D seismic reflection data, which has a peak frequency of 30 Hz, and is best used for comparison with the synthetic seismic and 2-D seismic reflection traces. The higher frequency (80 Hz) stack is valuable for resolving the tops, bottoms, and the heterogeneity within the units.

The top of the Fayette sandstone coincides with a 26 m (85 ft) thick sandstone bounded by shale. The sand unit produces a single low amplitude positive reflector at 270.67 ms, 322 m (1058 ft), but the higher frequency corridor stack shows the top and bottom of the sandstone. The Boyles Sandstone is separated into an upper and lower unit by a 30 m (100 ft) thick shale that is identified by a very high spike on the gamma ray log and produces a strong negative reflector on the synthetic trace (Figure 9). Directly below is a positive, high-amplitude reflector associated with the transition into the Lower Boyles Sandstone at 352.26 ms, 496 m (1627 ft). A

lithologic transition from sandstone to the underlying shale marks the top of the Parkwood Formation at 411.31 ms, 631 m (2071 ft). A single peak-trough-peak set makes up the entirety of the 76 m (250 ft) thick formation. The transition from trough to peak occurs because of a calcareous unit in the basal Parkwood that also corresponds to the top of the Bangor Limestone reflector at 444.55 ms, 707 m (2320 ft). Multiple peaks and troughs can easily be identified and correlated with the gamma ray log and sonic velocity to show formation heterogeneity.

The Bangor Limestone is the first of a series of strong amplitude reflections corresponding to the Hartselle Sandstone, Pride Mountain Formation, Tuscumbia Limestone, Chattanooga Shale, and the Red Mountain Formation. Strong reflectors are caused by the acoustic impedance changes between limestones, shales, and sandstones. A weak positive reflector is present at 478 ms, 797 m (2615 ft) on the synthetic at the top of the hydrocarbon-rich Hartselle Sandstone. A trough follows this when the Pride Mountain Shale is encountered at 489.15 ms, 824 m (2702 ft). Three dominant high amplitude peaks are the key tie points for the synthetic seismic (Figures 8 and 9). These reflectors correspond to the top of the Tuscumbia Limestone at 516.78 ms, 880 m (2888 ft), and the upper Red Mountain limestone at 543.34 ms, 952 m (3124 ft), and the Sequatchie Formation at 582.96 ms, 1057 m (3467 ft). The Chattanooga Shale at 539.44 ms, 941 m (3088 ft), and the middle Red Mountain silty shale at 552.12 ms, 1004 m (3294 ft), produce troughs in between the three main peaks. These distinct reflections result from contrasting lithologies and tuning effects.

There are significant differences in the corridor stacks between the top of the Tuscumbia Limestone and the top of the Red Mountain Formation. In the 80 Hz corridor stack, each of these formations, within that interval (e.g. Fort Payne Chert and the Chattanooga Shale), are detected. The Sequatchie Formation marks the top of a 1524 m (5000 ft) carbonate succession.

Within this large unit of carbonate rocks, there is a seismic peak that corresponds to the top of the Stones River Group at 614.2 ms, 1142 m (3746 ft), but the remainder of this section consists of low amplitude reflectors with good lateral continuity until the base of the Knox Group at approximately 1000 ms on the seismic reflection data. The Knox is also seen on the ZVSP at 1.14 seconds (Figure 8). It is characterized by laterally continuous, high amplitude reflectors that result from the abrupt change in acoustic impedance from dolomite to the calcareous shale of the Conasauga Formation.

6.0 DEPTH CONVERSION

By depth converting the 2-D seismic reflection profiles, one can not only make accurate interpretations but also extend volume calculations away from the well and accurately calculate dips of beds and structures. The study area has a low structural complexity, making a velocity model with continuous horizontal layers viable. In this model, each lithologic unit is defined using a velocity relationship as a function of burial depth (Marsden, 1989) that is constrained by the check-shot results. Specific velocity intervals were chosen based on lithology including the Parkwood Formation, Hartselle Sandstone, Tuscumbia Limestone, Lower Red Mountain Formation, Sequatchie Formation, and Conasauga Formation (Figures 11 and 12). It is especially important that horizons are picked accurately as velocities in the Black Warrior Basin can change abruptly among shale, coal, sandstone, limestone, and dolostones beds.

The velocity model, created in Petrel, is based on interval velocities from the sonic log calibrated using the check-shot data. Interval velocities from the sonic log calibrated check-shots were averaged for each unit and then input to the velocity model for each surface based on interpretations (Table 6). A polygon, containing the Plant Gorgas characterization well, was created around the two seismic lines. Surfaces were extrapolated from the interpreted seismic horizons using a convergent interpolation algorithm and a grid increment of 10 by 10 meters. A qualitative match between depth converted seismic surfaces and well tops provides evidence of an accurate velocity model (Figure 13).

Surface	Velocity (m/s)
Zero	0
Pottsville Formation	3763
Parkwood Formation	4715
Bangor Limestone	5419
Hartselle Sandstone	4146
Tuscumbia Limestone	5511
Lower Red Mountain Formation	5091
Sequatchie Formation	6300

Table 6: Interval velocities input to the velocity model. Velocities are applied to the unit overlying the given surface.

The first unit in the model is the heterogeneous Pennsylvanian Pottsville Formation, composed of interbedded sandstone, shale, and coal. This interval was assigned an average velocity of 3763 m/s. The underlying Parkwood Formation is composed of shale and limestone and has a velocity of 4715 m/s. The Bangor Limestone has a significantly higher velocity of 5419 m/s. The Hartselle Sandstone and Pride Mountain Shale make up 45.7 m (150 ft) of clastic material between these two limestone units and are assigned a significantly lower velocity of 4146 m/s. The Tuscumbia Limestone, Fort Payne Chert, Chattanooga Shale and upper Red Mountain Formation comprise a 128.3 m (421 ft) unit with a velocity of 5511 m/s, an increase in velocity from the overlying Hartselle/Pride Mountain unit. The Red Mountain is split into two units that are resolved on the seismic reflection data as distinct reflectors: the upper Red Mountain Formation is 33.5 m (110 ft) of limestone; the lower 68.5 m (225 ft) of the Red Mountain is silty shale. A surface was interpreted for the lower Red Mountain siltstone and a velocity of 5091 m/s was applied. A single velocity was applied to all units below the Red Mountain, including the Sequatchie Formation and the Knox Group. This velocity interval

consists of 1524 m (5000 ft) of limestone and dolomite that extends down to the Conasauga Formation, a strong continuous reflector that marks the first significant shale-limestone pair after the Knox Group. A velocity cannot be calculated for this unit because of a lack of data, but previous studies (Maher, 2002; Pearce, 2002; Gates, 2006) used wells that penetrated the entirety of the Cambrian-Ordovician carbonate unit and assigned a velocity of 6100 to 6400 m/s. The two depth converted lines in relation to the Gorgas well can be seen in three-dimensions in Figure 13.

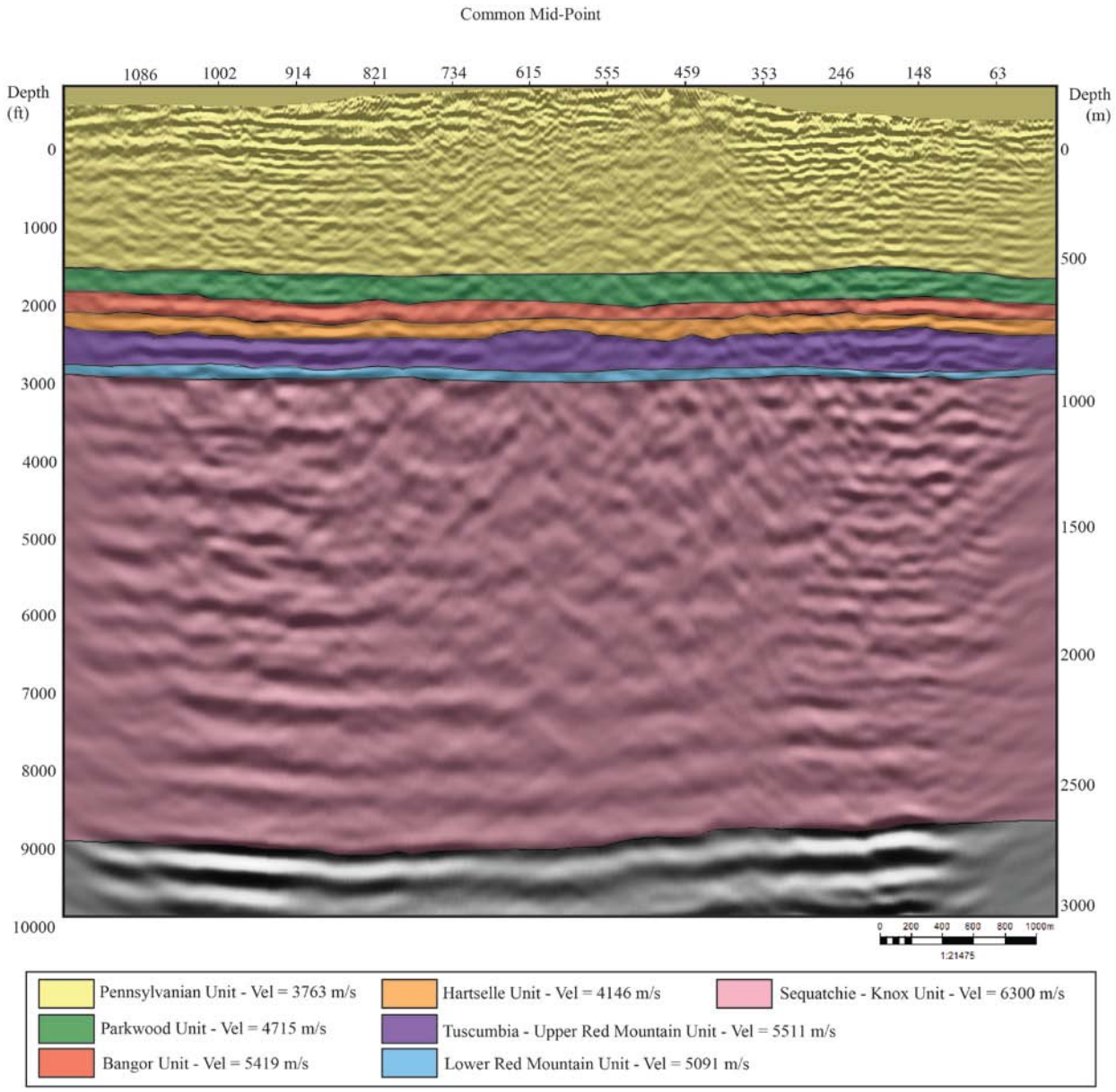

Figure 11: Depth converted seismic reflection data for Line 101. The vertical depth scale is given in feet (left) and meters (right) relative to mean sea level. CMP number is displayed along the horizontal axis. The velocity model used to convert time to depth is overlain on top of the seismic data with the average interval velocities for each unit indicated in the legend. All velocities are in meters per second (m/s).

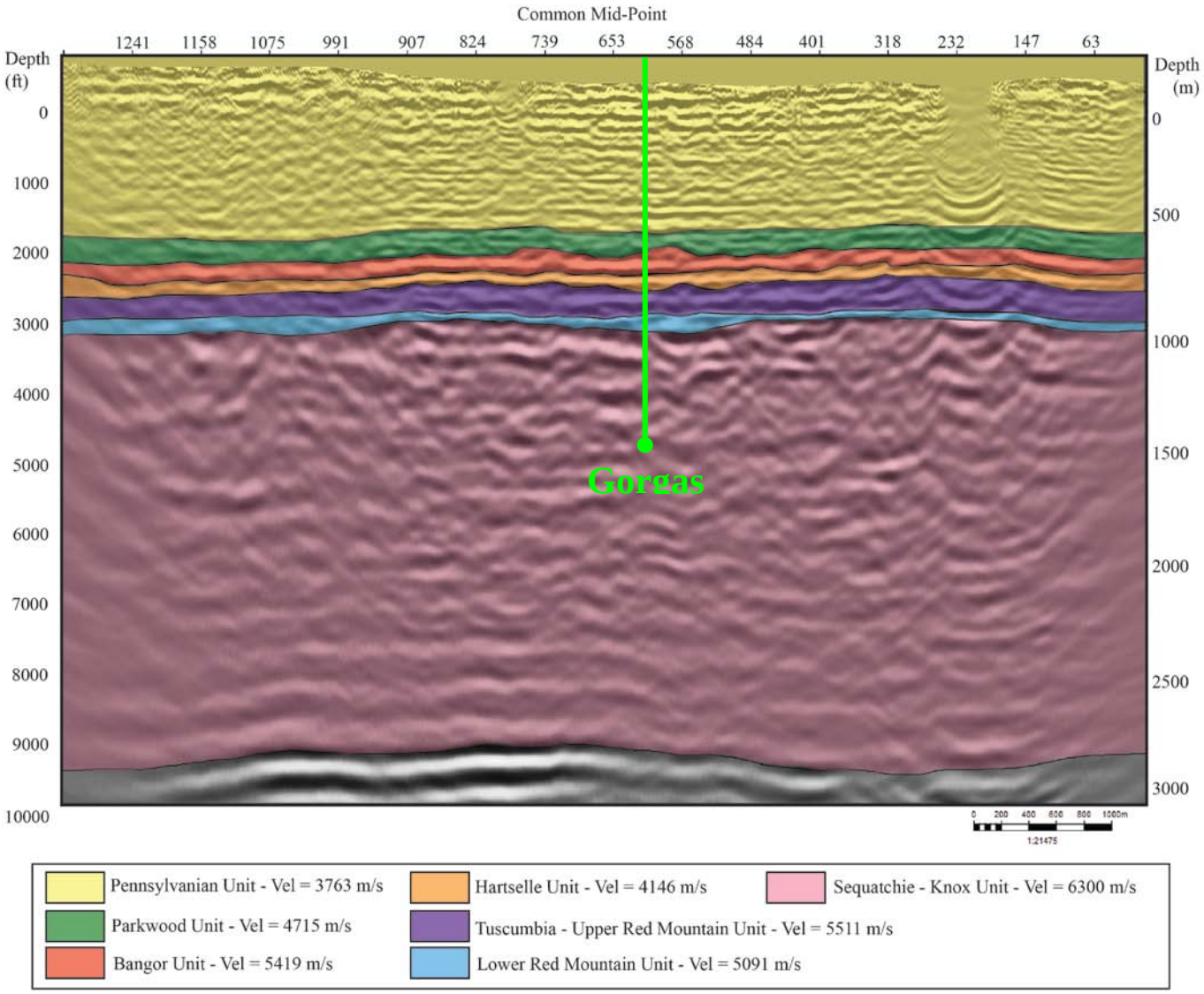

Figure 12: Depth converted seismic reflection data for Line 201. The vertical depth scale is given in feet (left) and meters (right) relative to mean sea level. CMP number is displayed along the horizontal axis. The velocity model used to convert time to depth is overlain on top of the seismic data with the average interval velocities for each unit indicated in the legend. All velocities are in meters per second (m/s).

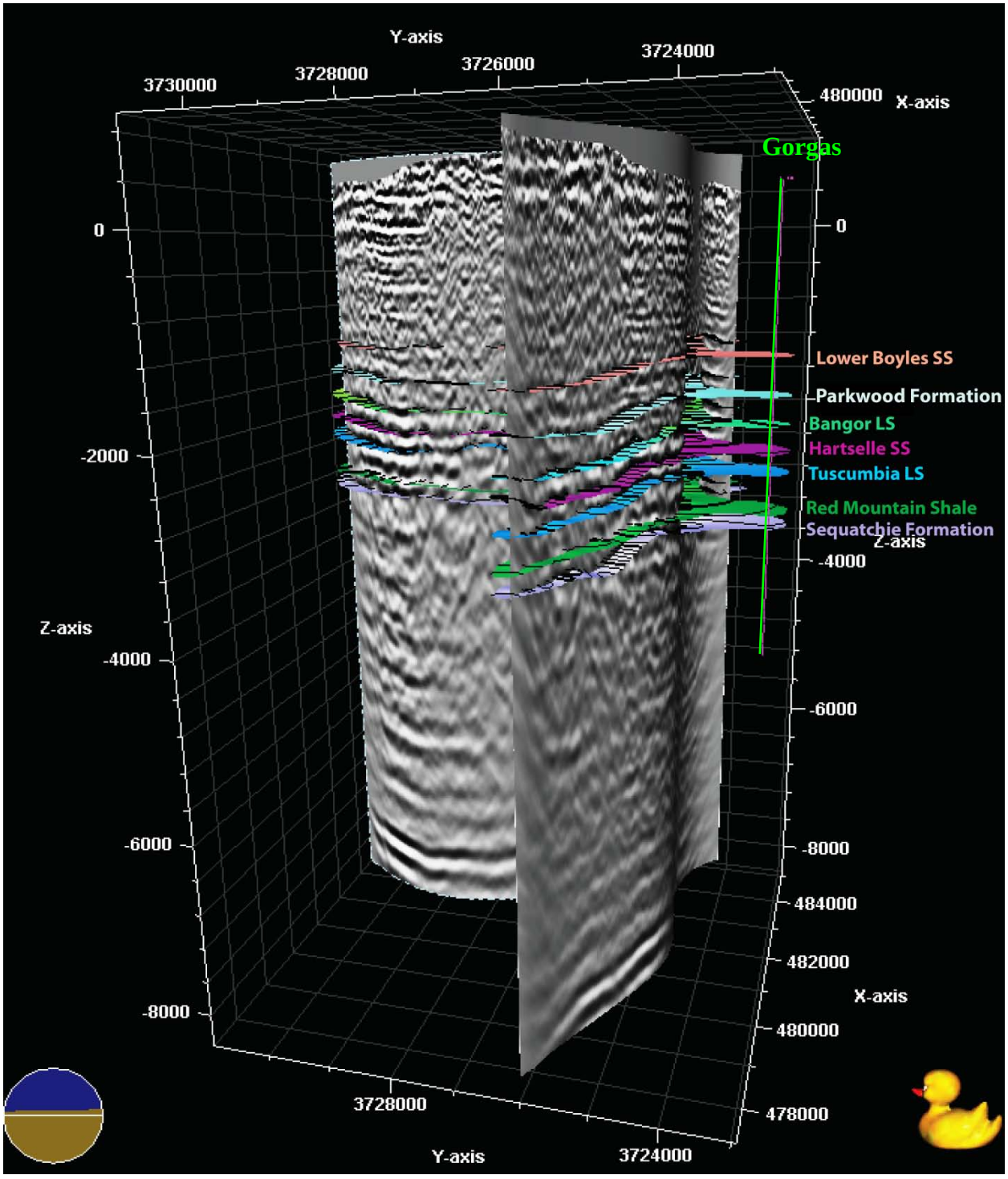

Figure 13: Three-dimensional view of depth converted Lines 101 and 201 with Gorgas #1 well located 0.8 miles south of Line 201. Seismic horizons are represented as 3-D surfaces that extend to the borehole. After the velocity model was applied, the depth-converted surfaces match the depth of correct formations from the borehole. The beak of the duck points north.

7.0 STORAGE CAPACITY

Capacity estimates for stacked saline aquifers and oil-rich reservoirs provide evidence that the Black Warrior Basin can store large quantities of anthropogenic CO_2. Target reservoirs suitable for geologic sequestration in the Black Warrior Basin are the Lower Boyles Sandstone, Hartselle Sandstone, Tuscumbia Limestone, and the Stones River Group limestone (Clark and Pashin, 2009). All target units are below the depth required for supercritical storage with the exception of the Pennsylvanian Boyles Sandstone in the lower Pottsville Formation, which would be injected with subcritical CO_2. Initial volumetric estimates are calculated from the data gathered on the geophysical well logs. The calculations are based on the hypothetical scenario that Southern Company captured and sequestered 10% of their average emissions from Plant Gorgas and injected the emissions at a constant rate for thirty years. The result defines the volume occupied at reservoir conditions encompassing a radius around the borehole after injection (Table 7). To calculate the CO_2 plume extent around the borehole, the following criteria were needed to estimate volume: depth of formation, thickness of unit, average porosity, reservoir temperature, reservoir pressure, and CO_2 saturation.

Plant Gorgas generates 7.5 megatons (Mt = 10^6 ton) of CO_2/year. Injecting ten percent of annual emissions equates to 0.75 megatons/year or roughly 2055 metric tons per day. Reservoir thickness, depth, and porosity were determined from geophysical well logs (Appendix III). Average porosities were estimated at 6% for the Lower Boyles Sandstone and 5% for the Hartselle Sandstone whereas an average porosity of the Tuscumbia Limestone was only 2% and even lower at 0.6% for the Stones Rivers Group. The low porosities are attributed to increased

cementation in the units under the Gorgas site in comparison to elsewhere in the basin. A more precise porosity evaluation of the limestone units can be determined in the future once a more detailed interpretation of core samples are completed by the Geological Survey of Alabama. A geothermal gradient of 25^{o} C/km and a pressure gradient of 10 MPa/km were used for the Black Warrior Basin (Carroll et al., 1995). Pressures and temperature were then used to determine the density of pure CO_2 (kg/m^3) at reservoir conditions for each of the units (Bryant, 2010). A more detailed report of values for individual reservoirs is provided in Appendix IV. The report provides values for the volume occupied by CO_2 at reservoir conditions and the necessary bulk volume of rock needed for storage.

The first steps in the calculation involve converting a given CO_2 output to volume using the density of CO_2 at reservoir conditions. The volume occupied by CO_2 is directly related to the density of CO_2 after injection. Density in this region can change drastically near the critical point of CO_2, which is caused by a phase change (E. Carlson, 2011, personal communication). Densities were derived using the graph in Figure 14 (Steven L. Bryant, personal communication, 2012), which shows a CO_2 density gradient using pressure and temperature gradients typical of the United States Gulf Coast (Bryant, 2010). Low, median, and high density (kg/m^3) values were derived for each unit (based on the accuracy of picking values from the graph): Lower Boyles Sandstone (120, 135, 145); Hartselle Sandstone (365, 400, 460); Tuscumbia Limestone (500, 515, 525); Stones River Group (545, 550, 560). Assuming the injection of CO_2 at a constant rate for 30 years using median density values, the CO_2 would occupy over 100 million cubic meters in the Lower Boyles sandstone and less than 50 million cubic meters in the deeper Stones River Group due to CO_2 density differences with these depths. The higher the density the less volume occupied. Using the volume occupied by CO_2 (V_{CO2}), porosity (Φ), and saturation of

CO_2 (S_{CO2}; assumed to be a constant 50% for all units; Bryant, 2010) one can then determine the bulk volume of rock required to store any desired amount of CO_2 (Equation 1).

Equation 1

$$V_{bulk} = V_{CO2} \times \frac{S_{CO2}}{\Phi}$$

Bulk rock volume has an inverse relationship with porosity; hence low porosity limestone requires a greater storage volume than the slightly more porous sandstone units. After 30 years the bulk volume of rock that will be saturated with CO_2 range from ~ 5,555,000,000 m^3 (± 600,000,000) in the Lower Boyles sandstone; ~ 2,245,000,000 m^3 (± 300,000,000) in the Hartselle Sandstone; ~ 4,220,000,000 m^3 (± 126,000,000) in the Tuscumbia Limestone; ~12,950,000,000 m^3 (± 230,000,000) in the Stones River Group limestone. Equation 2 is used to calculate the radius of the CO_2 plume (R_{CO2}) around the borehole using the calculated bulk volume and the thickness of the reservoir (h). These preliminary calculations will be enhanced by further studies (including core analysis and re-processing of the seismic data that are beyond the scope of this study).

Equation 2

$$R_{CO2} = \left(\frac{V_{bulk}}{h} \times \pi\right)^{1/2}$$

The radius of the predicted CO_2 plume around the borehole for the Lower Boyles sandstone is 3.615 km (2.25 miles) ± 0.22 km (0.14 miles), the Hartselle Sandstone is 5.19 km

(3.23 mile) ± 0.35 km (0.18 miles), the Tuscumbia Limestone is 4.70 km (2.92 miles) ± 0.07 km (0.04 miles), and the Stones River Group limestone is 7.2 km (4.47 miles) ± 0.06.5 km (0.04 miles; Table 7). Regional dip of the Black Warrior Basin is less than 1° SW (Figure 2) implying that an injected CO_2 plume would form symmetrical to slightly asymmetrical toward the northeast around the borehole (Petrusak et al., 2009).

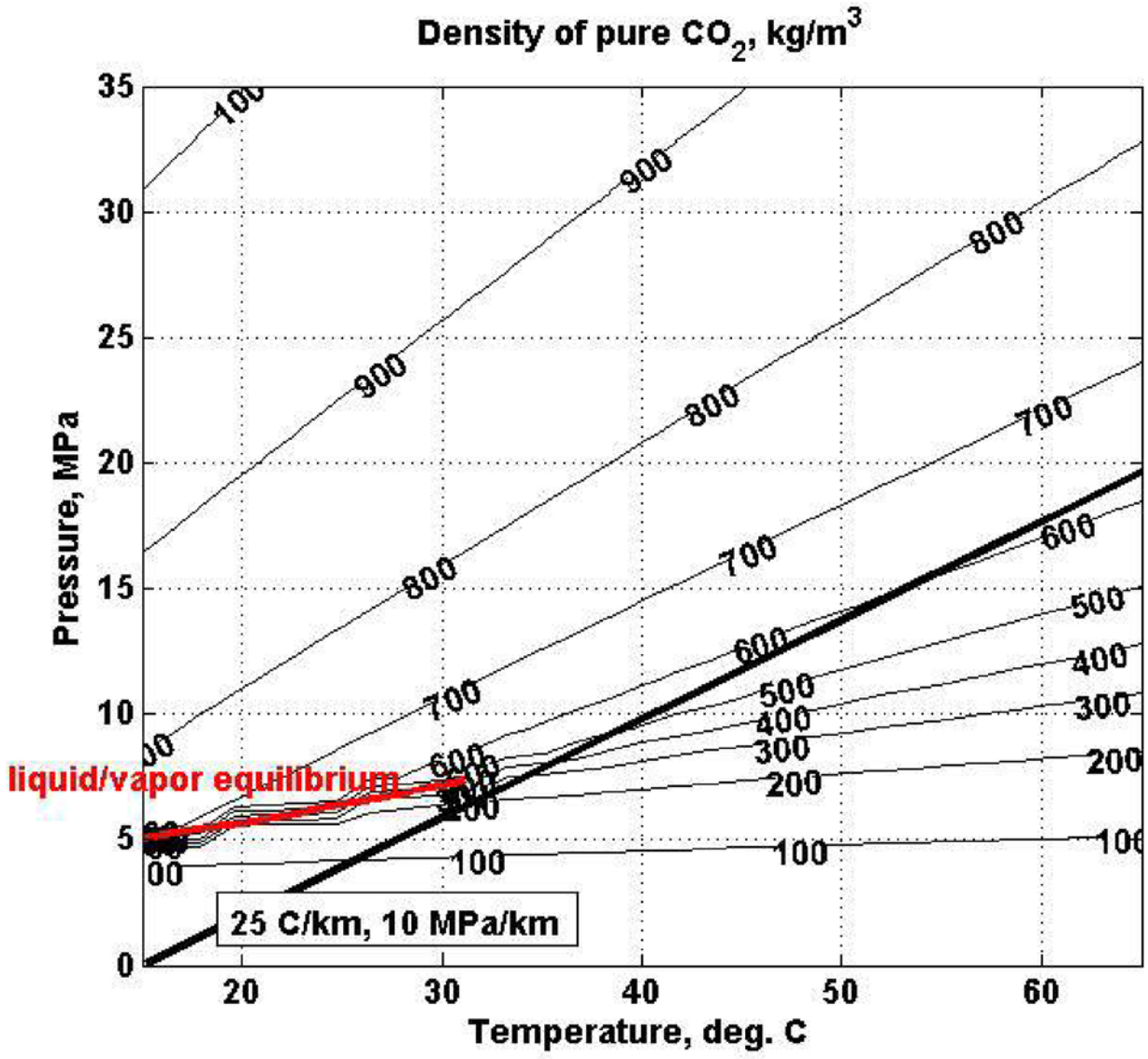

Figure 14: Plot of CO_2 density gradient using pressure and temperature gradients typical of the United States Gulf Coast (Bryant, 2010).

A generic diagram showing how the plume would behave in a reservoir is shown in Figure 15. The presence of oil and gas in several stacked reservoirs at the Gorgas site suggests that there are proven traps and seals. Multiple units, for example the Hartselle Sandstone and Tuscumbia Limestone, are reservoir quality and at the Gorgas site have an impermeable seal above them. The tight Bangor Limestone or siliceous cement in the upper section of the sandstone forms a seal for the Hartselle Formation. As for the Tuscumbia, either the overlying shales of the Pride Mountain Formation, or cementation within the Tuscumbia act as a seal. The prediction of the aerial extent of a CO_2 plume is based on preliminary data from geophysical well logs only. A more detailed core analysis and reservoir model will be the next step in better understanding injectivity and capacity of the geologic media. Reservoir simulations will help to visualize storage capacity, reservoir performance, fluid migration, and containment within saline zones while compensating for parameters such as geochemical interactions and discrete fracture networks propagation pathways.

Unit	Radius (km) after a 30 year period
Lower Boyles	3.615 ± 0.22 km
Hartselle	5.192 ± 0.35 km
Tuscumbia	4.695 ± 0.07 km
Stones River	7.199 ± 0.065 km

Table 7**:** Volumetric Estimates

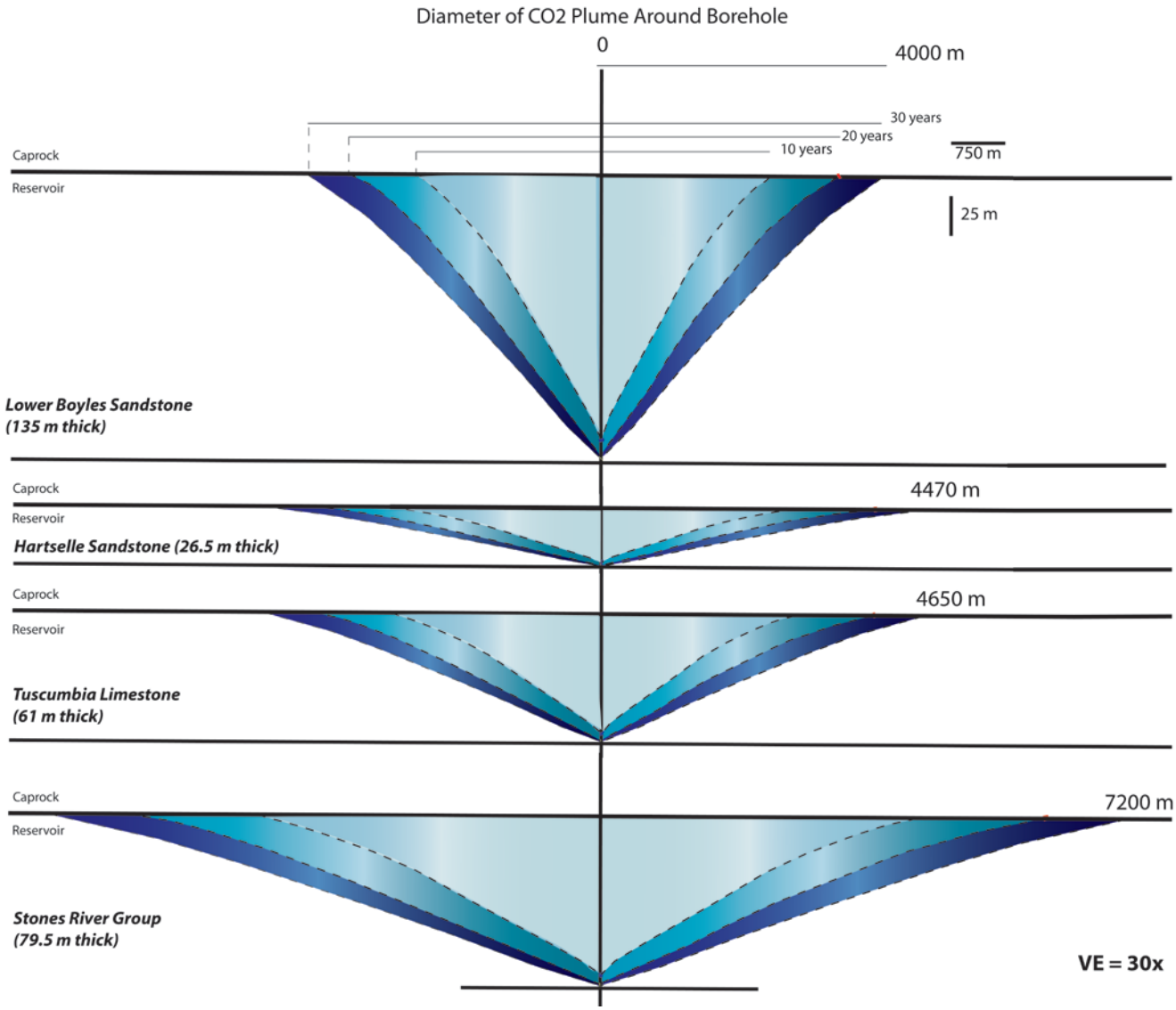

Figure 15: Diagram showing the growth of a CO_2 plume around the injection well over a span of thirty years.

8.0 DISCUSSION

Prior to collecting the data, little was known about the local geology underlying the Plant Gorgas area. After the 2-D seismic reflection data were processed, a gentle antiform with a symmetrical cuspate geometry was present at a depth of approximately 2743 m (9000 ft) on Line 201 in the lower Conasauga reflectors (Figure 12, centered between CMP 907 and 739) at approximately 1000 ms. The feature is not present on Line 101, which runs perpendicular to Line 201 that crosscuts the gently dipping anticline. It should be noted that this could be an artifact of early stage seismic processing, especially as the structure has an inverse relationship with the surface topography and reflectors are affected by noise and low fold on the sides of the structure at depth (Figure 6). The interpretation of this sequence of reflectors as the Conasauga Formation is based on several M. S. theses (Maher, 2002; Pearce, 2002; Gates, 2006) that provide interpretations of 2-D seismic reflection data and balanced cross-sections across the Appalachian Valley and Ridge province in northeastern Alabama. In that area, approximately 180 km northeast of Plant Gorgas on the Wills Valley Anticline, the Conasauga Formation is much shallower at ~609 m (2000 ft). Similar to our data, the interpreted Conasauga Formation is the next continuous high amplitude event below the thick Ordovician-Cambrian aged Knox carbonate unit.

The limbs of the anticline have an apparent dip of 3°. This anticlinal feature would aid in containment of a CO_2 plume by keeping it from migrating up-dip with the regional trend to the northeast. This is in contrast to the previous statement concerning the viability of Plant Miller's location for geologic sequestration. Plant Miller is a poor candidate for sequestration because it is located on the ramp of a fault-bend fold, which created steeper dipping beds that could create

problems tracking plume migration and is more likely to be highly fractured. The quality of the seismic data does not allow us to definitively state that the structure extends into the target reservoirs more than 1524 m (5000 ft) above. However, formations at Plant Gorgas were on average 60.9 m (200 ft) shallower than anticipated. The Ordovician Stones River Group was approximately ~90 m (300 ft) thinner than expected. The Cambrian-Ordovician Knox Group was approximately 259 m (850 ft) shallower than anticipated; the Copper Ridge dolomite was anticipated to be near ~1830 m (6000 ft) depth, but was encountered at 1372 m (4500 ft; J. Pashin, 2011, personal communication). The unexpected amounts of hydrocarbons in multiple units would suggest that the anticlinal feature seen at 2743 m (9000 ft) does affect the overlying units by creating a trap. Further evidence for the anticlinal structure affecting the units higher in the vertical succession is the unusually low porosities in the target reservoirs. It is normal to have high quartz cementation in anticlinal structures. Silica is easily transported in areas with gently folded stratigraphy due to a dynamic fluid flow allowing accumulation of a silica rich solution in the crest of the structure (Wood, 1984).

One scenario to explain the anticlinal structure seen on Line 201 would be an underlying southeast dipping blind thrust soling into the Conasauga Formation (Figure 16a). A breakdown of regional detachment surfaces by Thomas and Bayona (2002) suggest that if this were an anticline caused by the termination of a decollement, the displacement would most likely be in the Lower and Middle Cambrian strata inhibited by fine grained clastic rocks of the Rome and Conasauga formations (Unit 1 in their published work). A second scenario that could produce an anticline is a rollover structure above a basement cutting listric normal fault (Figure 16b). This fault would be out of plane of the 2-D seismic reflection profiles acquired for this project. In concurrence with basement faults in the basin, the strike of the theoretical fault could be

northwest-southeast dipping to the southwest. Alternatively, given the proximity to the Appalachian thrust front and the Birmingham graben system, this structure could be indicative of a reactivated fault related to Iapetan rifting (i.e. the Birmingham Graben System). Confirmation of this structure will require additional seismic data acquisition.

This study shows that multiple stacked saline aquifers below Plant Gorgas have the potential to provide long-term storage for CO_2 in the Black Warrior basin. Reservoirs, including the Hartselle Sandstone and the Tuscumbia Limestone may also be candidates for enhanced oil recovery (EOR) projects. The current quality of the available seismic data precludes confident fault picks, though faults are well documented in areas of past and present coal bed methane production (Pashin et al., 2001; Pashin et al., 2009; Groshong et al., 2010). The majority of faults in the basin are thin-skinned normal faults that are younger than the Pennsylvanian that sole to a detachment in the Pottsville Formation (Groshong et al., 2010). As the sequestration targets are in the deeper saline aquifers that are isolated by proven seals, evidenced by the hydrocarbons found in the characterization well, these shallow faults are of little concern. Further data collection west of the characterization site would help to ensure that no potential larger faults associated with reactivated faults related to Iapetan rifting could inhibit leakage would be worth investigating.

The Hartselle Sandstone was cored, and samples had a petroliferous odor and a blue to white fluorescence indicative of ~40^o API gravity oil, which is light enough to facilitate miscible CO_2 flooding. The presence of hydrocarbons suggests that a seal is in place that could serve as a seal for CO_2 after proper geochemical laboratory tests and mathematical simulations of mineral dissolution and precipitation have been performed. This may prove beneficial for the overall project due to a more mature permitting process and economic model for CO_2-EOR. Flooding

oil reservoirs with CO_2 has been a successful means of secondary or tertiary recovery since the early 1970's, but has yet to become routine practice because of the availability of anthropogenic CO_2. A combination of CO_2 sequestration and EOR is attractive to utility companies because it can offset the cost of capture, separation, and compression of carbon dioxide (Esposito, 2008). CO_2 injection can be continued after EOR operations have ceased. Anthropogenic CO_2 will enable further use of this technique and will ensure the growth of a pipeline infrastructure. Due to the extremely low porosities in these reservoirs, it is not clear whether injection can even be performed at this site, although some tight oil experiments may be feasible in the Hartselle Sandstone and the Tuscumbia Limestone.

The Lower Boyles Sandstone formation stands out as having potential for subcritical storage. This means the CO_2 would be stored at a pressure lower than 7.5 MPa (1,089 psi) and 26° C (79° F). Prior to performing these calculations, the Lower Boyles Sandstone had been considered too shallow for injection. The unit was only included in the estimations as a means to compare units with supercritical CO_2 potential to a unit with subcritical properties in an effort to show the importance of having CO_2 in a supercritical phase to maximize concentration. After the calculations were completed, the volumes for the Lower Boyles Sandstone were comparable with those in the Hartselle Sandstone, which is the unit favored for supercritical storage.

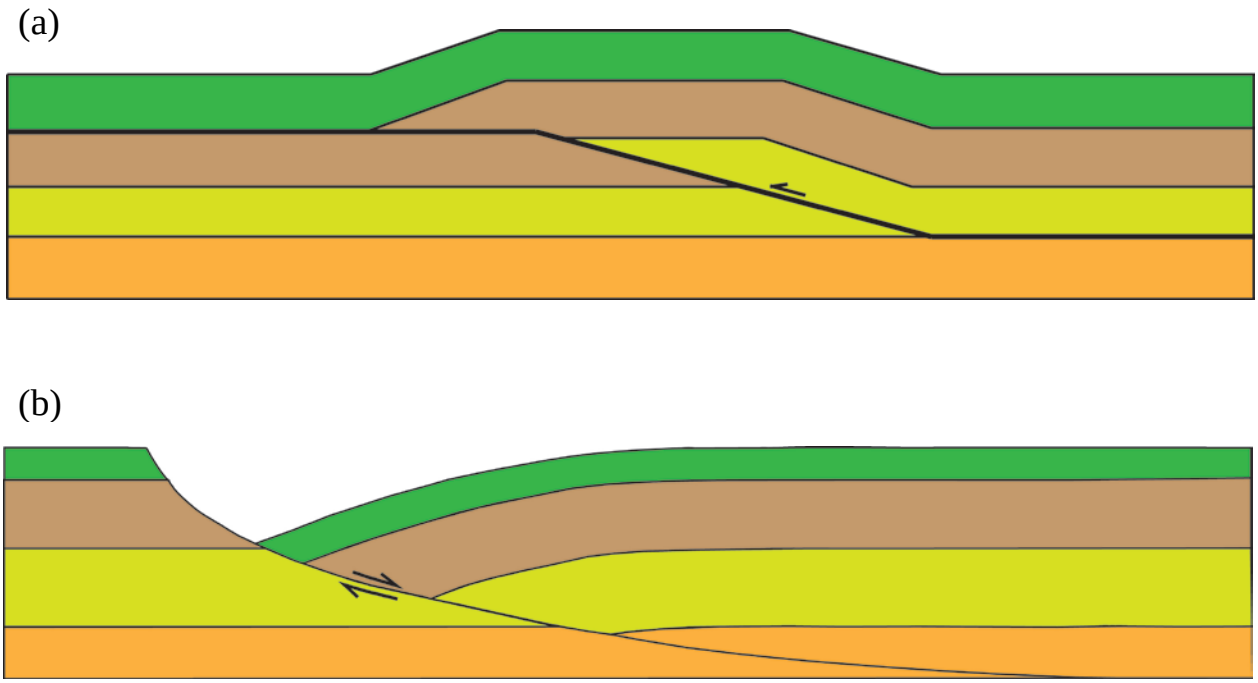

Figure 16: Scenarios used to explain anticline presence below Plant Gorgas. (a) A blind thrust soling into the Conasauga Formation. (b) A listric normal fault that creates a roll-over anticline in the hanging wall.

9.0 CONCLUSIONS

1) This study details the depth-time relationship for the stratigraphy tied to the Gorgas #1 well. The relationship is extrapolated beyond the characterization well using depth converted seismic reflection data.

2) Contrary to the baseline hypothesis that the area beneath Plant Gorgas has flat lying stratigraphy, an anticlinal structure is apparent on seismic reflection Line 201. This demonstrates that gentle folds are present to the west of the Sequatchie Anticline. Previous interpretations depict the Sequatchie Anticline as the furthest most thrust in the Black Warrior basin though this structure could be caused by another blind thrust further west than the Sequatchie Anticline (Thomas and Bayona, 2002; Thomas, 2007). It is possible that this structure originates from reactivation of faults that originally formed during Iapetan rifting. This finding attests to the need to collect more subsurface data in the area to further study the western limit of Alleghanian deformation.

3) No large-scale faults that could create CO_2 leakage pathways were identified in the seismic reflection profiles. Faults may be present in the Pottsville Formation; however, they were not resolvable due to the quality of the seismic data. These normal faults would sole into the detachment at the base of the Pottsville Formation seen throughout the basin (Groshong et al, 2010). Reprocessing of the data may reveal potential leakage pathways.

4) The anticlinal structure may provide a trapping mechanism for hydrocarbons. Increased cementation, commonly found associated with the crest of anticlinal structures, was abundant in core from the Gorgas #1 well. This indirectly provides evidence for the presence of the structure in the units being characterized. Cementation did have negative effects on porosity at the Plant Gorgas site, though it provides an additional sealing mechanism for potential reservoirs such as the Hartselle Sandstone and Tuscumbia Limestone units.

5) The Hartselle Sandstone is the only unit that is suited for injection at supercritical conditions. Although, porosity was considerably low (< 10%), after core analysis has been completed, the true permeability of the unit will be known to determine the true injectivity potential of the Hartselle Sandstone. Below the Hartselle Sandstone all units were well cemented and showed little to no visible porosity.

6) Hydrocarbons were discovered in the Fayette sandstone and Boyles sandstone members of the Pottsville Formation, the Hartselle Sandstone, and the Tuscumbia Limestone. Supplementary core analysis yielding suitable permeability and porosity values may impact the future of the area and the potential of sequestration and EOR activities.

7) Volumetric calculations for the Boyles and Hartselle Sandstones, and the Tuscumbia and Stones River Group limestones demonstrate they have the potential to store substantial amounts of CO_2 in the Black Warrior Basin. Assuming that 10% of Plant Gorgas's emissions can be sequestered over a thirty year period of injection, the Lower Boyles Sandstone CO_2 plume would extend to a radius of 3.615 km (2.25 miles) ± 0.22 km (0.14 miles) around the borehole. The

Hartselle Sandstone plume extends to a radius of 5.19 km (3.23 miles) ± 0.35 km (0.18 miles), around the borehole. The Tuscumbia Limestone plume extends to a radius of 4.70 km (2.92 miles) ± 0.07 km (0.04 miles), around the borehole. The Stones River Formation plume extends to a radius of 7.2 km (4.47 miles) ± 0.065 km (0.04 miles) around the borehole. It is recommended that the Hartselle Sandstone is the only unit that should be used to sequester CO_2 at a supercritical condition. Based on values derived from the volumetric calculations, the Lower Boyles sandstone also shows good potential for storage at subcritical conditions.

REFERENCES

Bachu, S., J. C. Shaw, and R. M. Pearson, 2004, Estimation of oil recovery and CO_2 storage capacity in CO_2 EOR incorporating the effect of underlying aquifers: Society of Petroleum Engineers Paper 89340, p. 1–13.

Beavers, W. M. and P. A. Boone, 1976, Depositional environments and petroleum potential of the asphaltic Hartselle Sandstone in North Alabama: Gulf Coast Associations of Geological Societies Transactions, v. 26, p 10-16.

Box, R., L. Maxwell and D. Loren, 2004, Excellent synthetic seismograms through the use of edited logs: Lake Borgne Area, Louisiana, U.S.: TLE, v. 23, no. 3, p. 218 – 223.

Bryant, S. L., 2010, CO_2 Injection for Geological Storage: Gulf Coast Association of Geological Sciences Meeting, Short Course no. 7.

Campbell, A., A. Fryer, and S. Wakeman, 2005, Vertical seismic profiles – more than just a corridor stack: TLE, v. 24, no. 7, p. 694 – 697.

Carroll, R. E., J. C. Pashin, and R. L. Kugler, 1995, Burial history and source-rock characteristics of Upper Devonian through Pennsylvanian strata, Black Warrior basin, Alabama: Alabama Geological Survey Circular 187, 29 p.

Chowns, T. M and F. K. McKinney, 1980, Depositional facies in Middle-Upper Ordovician and Silurian rocks of Alabama and Georgia: Geological Society of America, 1980 Field Trip No. 16, Guidebook, p. 323-348.

Clark, P. E. and J. C. Pashin, 2009, Site Characterization for CO_2 Storage from Coal-fired Power Facilities in the Black Warrior Basin of Alabama: Proposal in Response to DE-FOA-0000033 Recovery Act: Site Characterization of Promising Geologic Formations for CO_2 Storage: The University of Alabama, 43 p.

Cleaves, A.W. and F.W. Stapor, 1992, Mississippian (Chesterian) Sequence Stratigraphy in the Black Warrior Basin: Pride Mountain Formation (Lowstand Wedge) and Hartselle Sandstone (Transgressive Systems Tract), Gulf Coast Association of Geological Societies Transactions, v. 42, p. 683-696.

DiGiovanni, M., Jr., 1984, Stratigraphy and depositional environments of the lower Pride Mountain Formations (Upper Mississippian) in the Colbert County area, northwest Alabama, Master's thesis, The University of Alabama, Tuscaloosa, AL, 172 p.

Drahovzal, J. A., and T. L. Neathery, 1985, Lithostratigraphy of Upper Ordovician Strata in Alabama: Geological Survey of Alabama, Circular 124, 55 p.

Ettensohn, F. R. and J. C. Pashin, 1993, Mississippian stratigraphy of the Black Warrior basin and adjacent parts of the Appalachian basin: Evidence for flexural interaction between two foreland basins, ed. J. C. Pashin, New Perspectives on the Mississippian System of Alabama: Alabama Geological Society 30th Annual Field Trip Guidebook, 151 p.

Esposito, R. A., J. C. Pashin, and P. M. Walsh, 2008, Citronelle Dome: A giant opportunity for multizone carbon storage and enhanced oil recovery in the Mississippi Interior Salt Basin of Alabama: Environmental Geosciences, v. 15, no. 2, p. 53-62.

Faust, L. Y., 1953, A Velocity Function Including Lithologic Variation: Geophysics, v. 18, p. 271-297.

Ferrill, B. A, 1989, Middle Cambrian to Lower Mississippian Synsedimentary Structures in the Appalachian Fold-Thrust Belt in Alabama and Georgia, Ph.D. dissertation, The University of Alabama, Tuscaloosa, AL, 270 p.

Gates, M. G., 2006, Structure of Wills Valley Anticline in the vicinity of Mentone, Alabama, Master's thesis, The University of Alabama, Tuscaloosa, AL, 46 p.

Gochioco, L. M., 1991, Tuning effect and interference reflections from thin beds and coal seams: Geophysics, v. 56, no. 8, p. 1288-1295.

Groshong, R. H., Jr., J. C. Pashin, and M. R. McIntyre, 2010, Structural controls on fractured coal reservoirs in the southern Appalachian Black Warrior foreland basin: Journal of Structural Geology, v. 31, p. 874-886.

Hazeldine, R. S., 2009, Carbon Capture and Storage: How Green Can Black Be?: Science, v. 325, p. 1674-1652.

Kaldi, J. G., C. M. Gibson-Poole, and T. H. D. Payenberg, 2009, Geological input to selection and evaluation of CO2 geosequestration sites, *in* M. Grobe, J.C. Pashin, and R.L. Dedge, eds., Carbon dioxide sequestration in geological media—State of the science: AAPG Studies in Geology 59, p. 5 – 16.

Kallweit, R. S. and L. C. Wood, 1982, The limits of resolution of zero-phase wavelets: Geophysics, v. 47, no.7, p. 1035-1046.

Kim, D. Y., 1964, Synthetic velocity log (abs.): 33rd Annual International SEG Meeting, New Orleans, LA.

Linari, V., 2004, A practical approach to well-seismic data calibration: The Leading Edge, vol. 23, p. 774-755.

Liner, C. L., 2004, Elements of 3D Seismology, Second Edition: Tulsa, OK, PennWell Corporation, 608 p.

Maher, C. A., 2002, Structural deformation of the southern Appalachians in the vicinity of the Wills Valley Anticline, Northeast Alabama, Master's thesis, The University of Alabama, Tuscaloosa, AL, 45 p.

Marsden, D., 1989, I. Layer cake depth conversion: Geophysics: The Leading Edge, v. 8, p. 10-14.

Miall, A. D., 2008, The Sedimentary Basins of the United States and Canada, Elsevier, v. 5, p. 1-105.

Moores, E. M. and R. J. Twiss, 1992, Structural Geology: New York, W. H. Freeman and Co., 532 p.

Murphy, J. B., G. Gutierrez-Alonso, R. D. Nance, J. Fernandez-Suarez, J. D. Keppie, C. Quesada, R. A. Strachan, and J. Dostal, 2006, Origin of the Rheic Ocean: Rifting along a Neoproterozoic suture?: Geology, v. 34, no. 5, p. 325 -328.

Orr, F. M. Jr., 2009, Onshore geologic storage of CO_2: Science Magazine, v. 325, p. 1656-1657.

Osborne, W. E. and D. E. Raymond, 1992, The Knox Group in the Appalachian fold-thrust belt and Black Warrior Basin of Alabama: Stratigraphy and Petroleum Exploration: Geological Survey or Alabama, Circular 162, p. 34.

Pashin, J. C., 1993, Tectonics, paleoceanography, and paleoclimate of the Kaskaskia sequence in the Black Warrior Basin of Alabama, *in* Pashin, J. C., ed. New perspectives on the Mississippian System of Alabama (guidebook, Alabama Geological Society 30th annual field trip): Alabama Geological Society, 28 p.

Pashin, J. C., 1994, Cycles and stacking Patterns in Carboniferous Rocks of the Black Warrior Foreland Basin: Alabama Geological Survey Reprint Series 103, p. 559-563.

Pashin, J. C, 2008, Gas Shale Potential of Alabama: Geological Survey of Alabama, Tuscaloosa, AL, 2008 International Coalbed & Shale Gas Symposium Proceedings, p. 1-13.

Pashin, J. C., R. H. Groshong Jr., and R. E. Carroll, 2001, Enhanced coalbed methane recovery through sequestration of carbon dioxide: potential for a market-based environmental solution in the Black Warrior basin of Alabama: Washington, D.C., U.S. Department of Energy, National

Energy Technology Laboratory, First National Conference on Carbon Sequestration Proceedings, DOE/NETL-2001/1144, CD-ROM.

Pashin, J. C., M. R. McIntyre, R. E. Carroll, R. H. Groshong Jr., and R. M. Bustin, 2009, Carbon sequestration and enhanced recovery potential of mature coalbed methane reservoirs in the Black Warrior Basin, in M. Grobe, J. C. Pashin, and R. L. Dodge, eds., Carbon dioxide sequestration in geological media—State of the science: AAPG Studies in Geology 59, p. 125 – 147.

Pashin, J. C. and R. A. Gastaldo, 2009, Carboniferous of the Black Warrior basin, in Greb., S. F., and Chesnut, D. R., eds., Carboniferous Geology and Biostratigraphy of the Appalachian Basin: Kentucky Geological Survey Special Publication 10, p. 10-21.

Pashin, J. C., R. L. B. Grace, and D. C. Kopaska-Merkel, 2010, Devonian shale plays in the Black Warrior basin and Appalachian thrust belt of Alabama: Tuscaloosa, Alabama, University of Alabama, College of Continuing Studies, 2010 International Coalbed & Shale Gas Symposium Proceedings, paper 1016, 20 p.

Pawlewicz, M. J. and J. R. Hatch, 2007, Petroleum assessment of the Chattanooga Shale/Floyd Shale–Paleozoic Total Petroleum System, Black Warrior Basin, Alabama and Mississippi, *in* Hatch, J. R., and Pawlewicz, M. J., compilers, Geologic assessment of undiscovered oil and gas resources of the Black Warrior Basin Province, Alabama and Mississippi: U.S. Geological Survey Digital Data Series DDS–69–I, chap. 3, 23 p.

Pearce, P. J., 2002, Seismic interpretation and structural restoration of a transect from Murphree's Valley to the Talladega National Forest: The Appalachian Valley and Ridge of Alabama, Master's thesis, The University of Alabama, Tuscaloosa, AL, 51 p.

Petrusak, R., D. Riestenberg, P. Goad, K. Schepers, J. C. Pashin, R. Esposito, and R. Tautz, 2009, World class CO_2 sequestration potential in saline formations, oil and gas fields, coal, and shale: the US Southeast Regional Carbon Sequestration Partnership has it all: Society of Petroleum Engineers International Conference, SPE 126619, p. 1-18.

Raymond, D. E., 1991, New subsurface information on Paleozoic stratigraphy of the Alabama fold and thrust belt an d the Black Warrior Basin: Tuscaloosa, AL, Geological Survey of Alabama, Bulletin 143, 185 p.

Robinson, D. M**.,** M. G. Gates, and A. M. Goodliffe, 2009, Structure of the Wills Valley Anticline, Alabama: Gulf Coast Association of Geological Societies Transactions, v. 59, p. 663-671.

Rudman, A. J., J. F. Whaley, R. F. Blakely, and M. E. Biggs, 1975, Transformation of resistivity to pseudo velocity logs: American Association of Petroleum Geologists Bulletin, v. 59, p.1151-1165.

Ryder, R. T., 1987, Oil and Gas Resources of the Black Warrior Basin, Alabama and Mississippi: U. S. Geological Survey, report 87-450X, 25 p.

Scotese, C. R., and J. Golonka, 1992, PALEOMAP paleogeographic atlas: University of Texas-Arlington, Department of Geology, PALEOMAP Progress Report 20, 1 sheet.

Sheriff, R. E., 1999, Encyclopedic Dictionary of Exploration Geophysics, Third Edition: Society of Exploration Geophysicists, 384 p.

Smith, J. H., 2007, A method for calculating pseudo sonics from e-logs in a clastic geologic setting: Gulf Coast Association of Geological Societies Transactions, v. 57, p. 1-4.

Smith, S. A., J. A. Sorensen, E. N. Steadman, J. A. Harju, and D. W. Fischer, 2009, Estimates of CO2 storage capacity in selected oil fields of the northern Great Plains region of North America, in M. Grobe, J. C. Pashin, and R. L. Dodge, eds., Carbon dioxide sequestration in geological media—State of the science: AAPG Studies in Geology 59, p. 87– 97.

Stark, A., 2008, Seismic Methods and Applications: A Guide for the Detection of Geologic Structures, Earthquake Zones and Hazards, Resource Exploration, and Geotechnical Engineering: BrownWalker Press, 411 p.

Thomas, W. A., 1988, The Black Warrior Basin, *in* Sloss, L.L., ed., Sedimentary cover – North American craton. Boulder, Colorado, Geological Society of America, The Geology of North America, v. D-2, p. 471-492.

Thomas, W. A., 1989, The Appalachian-Ouachita orogen beneath the Gulf Coastal Plain between the outcrops in the Appalachian and Ouachita Mountains, *in* Hatcher, R. D. Jr., W. A. Thomas, and G. W. Viele, ed., The Appalachian-Ouachita Orogen in the United States. Boulder, Colorado, Geological Society of America, The Geology of North America, v. F-2, p. 537-554.

Thomas, W. A., 2004, Genetic relationship of rift-stage crustal structure, terrain accretion, and foreland tectonics along the south Appalachian – Ouachita orogen: Journal of Geodynamics, v. 37, p. 549-563.

Thomas, W. A., 2006, Tectonic inheritance at a continental margin: GSA Today, v. 16, no. 2, p. 4-11.

Thomas, W. A., 2007, Role of the Birmingham basement fault in thin-skinned thrusting of the Birmingham anticlinorium, Appalachian thrust belt in Alabama: American Journal of Science, v. 307, p. 42-62.

Thomas, W. A., and G. H. Mack, 1982, Paleogeographic relationship of a Mississippian barrier-island and shelf-bar system (Hartselle Sandstone) in Alabama to the Appalachian-Ouachita orogenic belt: Geological Society of America Bulletin, v. 93, p. 6-19.

Thomas, W. A., B. A. Ferrill, J. L. Allen, W. E. Osborne, and D. E. Leverett, 1991, Synorogenic clastic-wedge stratigraphy and subsidence history of the Cahaba Synclinorium and the Black Warrior foreland basin, *in* Thomas, W. A., and Osborne, W. E., eds., Mississippian-

Pennsylvanian tectonic history of the Cahaba Synclinorium (guidebook, Alabama Geological Society 28th annual field trip): Alabama Geological Society, p. 37-39.

Thomas, W. A., and B. M. Whiting, 1994, Three-dimensional controls on subsidence of a foreland basin associated with a thrust-belt recess: Black Warrior basin, Alabama and Mississippi: Geology, v. 22, p. 727-730.

Thomas, W. A., and G. Bayona, 2002, Palinspastic restoration of the Anniston transverse zone in the Appalachian thrust belt, Alabama: Journal of Structural Geology, v. 24, no. 4, p. 797-826.

Turcotte, D. L. and G. Schubert, 2002, Geodynamics, Second Edition: New York, NY, Cambridge University Press, 456 p.

Watts, A. B., 1992, The effective elastic thickness of the lithosphere and the evolution of foreland basins: Basin Research, v. 4, p. 169-178.

Wilson, G. V., 1987, Characteristics and resource evaluation of the asphalt and bitumen deposits of northern Alabama, Geological Survey of Alabama Bulletin, v. 111, 109 p.

Wood, J. R., 1984, A model for porosity reduction by quartz cementation in anticlinal structures: Abstract: CSPG Special Publications, p.566.

Zhaowen, L. D., Minngzhe, L. Shuliang, and S. Haung, 2006, CO_2 sequestration in depleted oil and gas reservoirs – caprock characterization and storage capacity: Energy Conservation and Management, v. 47, p. 1372-1382.

APPENDIX I

Appendix I (a)

CHECK-SHOT REPORT

SRD = Seismic Reference Datum, OWT = One-way travel time, KB = Kelly Bushing, RMS = Root mean squared.

Client and Well Information
Company: Alabama Power Company
Well: Gorgas #1
Field: Wildcat
County: Walker
State: Alabama
API Number: NA
Logging Date: 20-Sep-2011

Survey Information
SRD: 800.0 ft **KB elevation:** 389.84 ft **GL elevation:** 376.16 ft
Source Type: Vibroseis
Source Depth below KB: 13.74 ft
Source Distance from Wellhead: 162.0 ft
Source Azimuth from North: 345.0 deg
Velocity of Medium (Source to Sensor): 15000 ft/s
Velocity of Medium (Source to SRD): 15000 ft/s

LEVEL NUMBER FROM SRD	**VERTICAL** DEPTH FROM (owt)	**MEASURED** DEPTH KB (owt)	**OBSERVED** TRAVEL TIME	**VERTICAL** TRANSIT TIME-SRD	**ACOUSTIC** AVERAGE VELOCITY	**ACOUSTIC** RMS VELOCITY
ft	ft	s	s	ft/s	ft/s	ft/s
1	0	-484	0			
2	833.9	349.9	0.0517	0.0798	10456	10456
3	883.9	399.9	0.0546	0.0835	10585	10602
4	933.9	449.9	0.0582	0.0877	10648	10667
5	984	500	0.0619	0.0919	10709	10731
6	1034	550	0.0656	0.096	10776	10801
7	1084	600	0.0689	0.0995	10893	10934
8	1134	650	0.0724	0.1033	10974	11021
9	1184	700	0.0759	0.107	11069	11126
10	1234	750	0.0799	0.1112	11100	11156
11	1284	800	0.0838	0.1152	11148	11205
12	1334	850	0.0878	0.1193	11180	11235
13	1384	900	0.0914	0.123	11252	11314

14	1434	950	0.0951	0.1268	11306	11369
15	1483.9	999.9	0.0989	0.1307	11351	11415
16	1533.9	1049.9	0.1027	0.1346	11392	11456
17	1583.9	1099.9	0.1063	0.1383	11455	11524
18	1633.9	1149.9	0.1097	0.1418	11524	11599
19	1683.9	1199.9	0.1132	0.1453	11590	11669
20	1733.9	1249.9	0.1165	0.1486	11664	11752
21	1783.9	1299.9	0.12	0.1522	11719	11810
22	1833.9	1349.9	0.1235	0.1557	11776	11871
23	1883.8	1399.8	0.1271	0.1593	11823	11919
24	1933.8	1449.8	0.1306	0.1629	11868	11965
25	1983.8	1499.8	0.1342	0.1665	11913	12012
26	2033.8	1549.8	0.1379	0.1703	11942	12039
27	2083.9	1599.9	0.1416	0.174	11978	12076
28	2133.9	1649.9	0.1452	0.1776	12015	12113
29	2183.9	1699.9	0.1485	0.181	12068	12170
30	2233.9	1749.9	0.1518	0.1842	12126	12233
31	2284.1	1800.1	0.1548	0.1873	12192	12308
32	2334.1	1850.1	0.1582	0.1907	12241	12359
33	2384.1	1900.1	0.1612	0.1938	12303	12428
34	2434.1	1950.1	0.1646	0.1972	12343	12469
35	2483.5	1999.5	0.168	0.2005	12384	12512
36	2533.5	2049.5	0.1713	0.2039	12423	12553
37	2583.5	2099.5	0.1748	0.2075	12453	12582
38	2633.5	2149.5	0.1779	0.2106	12508	12642
39	2683.8	2199.8	0.1816	0.2142	12528	12660
40	2733.8	2249.8	0.1847	0.2174	12577	12714
41	2784.1	2300.1	0.1882	0.2209	12605	12741
42	2834.1	2350.1	0.1911	0.2238	12665	12810
43	2884.1	2400.1	0.194	0.2267	12723	12875
44	2934.1	2450.1	0.1965	0.2292	12799	12969
45	2984	2500	0.1993	0.232	12860	13039
46	3033.8	2549.8	0.2022	0.2349	12916	13101
47	3084	2600	0.2053	0.238	12959	13147
48	3134	2650	0.2082	0.241	13006	13197
49	3184	2700	0.2115	0.2442	13036	13227
50	3234	2750	0.2146	0.2474	13074	13266
51	3269.1	2785.1	0.217	0.2498	13088	13278
52	3384	2900	0.2263	0.2591	13061	13246
53	3434	2950	0.2293	0.2621	13104	13292
54	3484	3000	0.232	0.2648	13157	13352

55	3534	3050	0.2346	0.2674	13218	13425
56	3584	3100	0.2373	0.2701	13267	13480
57	3634	3150	0.24	0.2728	13323	13545
58	3684	3200	0.2429	0.2758	13359	13583
59	3734	3250	0.2456	0.2784	13411	13641
60	3783.9	3299.9	0.2484	0.2813	13453	13686
61	3833.9	3349.9	0.2513	0.2841	13495	13732
62	3884	3400	0.2543	0.2872	13524	13761
63	3934	3450	0.2574	0.2902	13555	13793
64	3983.9	3499.9	0.2603	0.2931	13590	13829
65	4033.9	3549.9	0.2632	0.296	13626	13867
66	4083.9	3599.9	0.266	0.2989	13664	13907
67	4133.9	3649.9	0.2687	0.3016	13708	13955
68	4183.9	3699.9	0.2715	0.3044	13746	13996
69	4233.9	3749.9	0.2741	0.307	13790	14046
70	4283.9	3799.9	0.2769	0.3098	13829	14088
71	4333.9	3849.9	0.2794	0.3123	13877	14142
72	4384	3900	0.2819	0.3148	13925	14198
73	4434	3950	0.2844	0.3173	13973	14253
74	4484	4000	0.287	0.3199	14019	14305
75	4534	4050	0.2894	0.3223	14066	14358
76	4584	4100	0.2919	0.3248	14111	14410
77	4634	4150	0.2943	0.3272	14162	14470
78	4684	4200	0.2968	0.3297	14207	14521
79	4734	4250	0.2991	0.332	14258	14581
80	4784	4300	0.3015	0.3344	14306	14637
81	4834	4350	0.3039	0.3368	14353	14691
82	4884	4400	0.3063	0.3392	14399	14743
83	4934	4450	0.3087	0.3417	14441	14791
84	4984	4500	0.3112	0.3441	14484	14839
85	5034	4550	0.3136	0.3466	14526	14885
86	5084	4600	0.316	0.3489	14570	14935
87	5134	4650	0.3183	0.3512	14618	14991
88	5184	4700	0.3206	0.3535	14663	15044
89	5234	4750	0.3229	0.3559	14708	15094
90	5284	4800	0.3253	0.3582	14750	15142
91	5334	4850	0.3276	0.3606	14793	15191

Appendix I (b).

VELOCITY REPORT

SRD = Seismic Reference Datum, OWT = One-way travel time, KB = Kelly Bushing, RMS = Root mean squared

Client and Well Information
Company: Alabama Power Company
Well: Gorgas #1
Field: Wildcat
County: Walker
State: Alabama
API Number: NA
Logging Date: 20-Sep-2011

Survey Information
SRD: 800.0 ft **KB elevation:** 389.84 ft **GL elevation:** 376.16 ft
Source Type: Vibroseis
Source Depth below KB: 13.74 ft
Source Distance from Wellhead: 162.0 ft
Source Azimuth from North: 345.0 deg
Velocity of Medium (Source to Sensor): 15000 ft/s
Velocity of Medium (Source to SRD): 15000 ft/s

TWO WAY TRAVEL TIME FROM SRD (ms)	MEASURED DEPTH FROM KB (ft)	VERTICAL DEPTH FROM SRD (ft)	AVERAGE VELOCITY SRD/GEO (ft/S)	RMS VELOCITY (ft/s)	INTERVAL VELOCITY (ft/s)
0	-410.2	0	10153	10153	10153
10	-359.4	50.8	10153	10153	10153
20	-308.6	101.5	10153	10153	10153
30	-257.9	152.3	10153	10153	10153
40	-207.1	203.1	10153	10153	10153
50	-156.3	253.8	10153	10153	10153
60	-105.6	304.6	10153	10153	10153
70	-54.8	355.4	10153	10153	10153
80	-4	406.1	10153	10153	10153
90	46.7	456.9	10153	10153	10153
100	97.5	507.7	10153	10153	10153
110	148.3	558.4	10153	10153	10153
120	199	609.2	10153	10153	10153
130	249.8	660	10153	10153	10153
140	300.6	710.7	10153	10153	10215

150	351.6	761.8	10156	10157	12927
160	416.3	826.4	10331	10354	11925
170	475.9	886.1	10424	10453	12157
180	536.7	946.9	10520	10554	13590
190	604.6	1014.8	10682	10737	13294
200	671.1	1081.3	10812	10879	12687
210	734.5	1144.7	10902	10974	12311
220	796.1	1206.3	10966	11041	13062
230	861.4	1271.6	11057	11140	12724
240	925	1335.2	11126	11212	12584
250	988	1398.1	11185	11271	12574
260	1050.8	1461	11238	11327	14774
270	1124.7	1534.9	11369	11474	14458
280	1197	1607.1	11479	11595	14279
290	1268.4	1678.5	11576	11700	12725
300	1332	1742.2	11614	11738	13538
310	1399.7	1809.9	11676	11801	14065
320	1470	1880.2	11751	11879	14573
330	1542.9	1953	11837	11970	11817
340	1602	2012.1	11836	11966	14797
350	1676	2086.1	11921	12058	15933
360	1755.6	2165.8	12032	12183	15117
370	1831.2	2241.4	12116	12272	15922
380	1910.8	2321	12216	12382	14520
390	1983.4	2393.6	12275	12444	15970
400	2063.3	2473.4	12367	12545	15116
410	2138.8	2549	12434	12615	14554
420	2211.6	2621.8	12485	12667	15032
430	2286.8	2696.9	12544	12733	16820
440	2370.9	2781	12641	12845	19290
450	2467.3	2877.5	12789	13024	17628
460	2555.5	2965.6	12894	13143	16418
470	2637.6	3047.7	12969	13222	15886
480	2717	3127.1	13030	13284	13607
490	2785	3195.2	13042	13292	11655
500	2843.3	3253.5	13014	13261	13265
510	2909.6	3319.8	13019	13274	19201
520	3005.6	3415.8	13138	13413	18124
530	3096.2	3506.4	13232	13517	17084
540	3181.7	3591.8	13303	13593	19468

550	3279	3689.2	13415	13723	16533
560	3361.7	3771.8	13471	13780	15905
570	3441.2	3851.4	13514	13820	17503
580	3528.7	3938.9	13582	13893	18185
590	3619.6	4029.8	13661	13977	18629
600	3712.8	4122.9	13743	14067	18742
610	3806.5	4216.7	13825	14157	19823
620	3905.6	4315.8	13922	14267	19669
630	4004	4414.1	14013	14369	20234
640	4105.1	4515.3	14110	14479	20493
650	4207.6	4617.7	14209	14591	20979
660	4312.5	4722.6	14311	14709	20600
670	4415.5	4825.6	14405	14814	19738
680	4514.2	4924.3	14484	14898	20772
690	4618	5028.2	14575	15000	21209
700	4724.1	5134.2	14669	15107	21204
710	4830.1	5240.3	14762	15210	

APPENDIX II

WIRELINE LOG DEFINITIONS

Curve Name	Units	Description
1WAY	μsec	One-Way Travel Time From Surface To Depth
AAMP		Average Amplitude
ABND	MV	Amplitude - Borehole - Near Detector
AF10	OHMM	Array Induction Four Foot Resistivity A1
AF20	OHMM	Array Induction Four Foot Resistivity A2
AF30	OHMM	Array Induction Four Foot Resistivity A3
AF60	OHMM	Array Induction Four Foot Resistivity A6
AF90	OHMM	Array Induction Four Foot Resistivity A9
AFCO	MM/M	Array Induction Four Foot Conductivity
AO10	OHMM	Array Induction One Foot Resistivity A10
AO20	OHMM	Array Induction One Foot Resistivity A20
AO30	OHMM	Array Induction One Foot Resistivity A30
AO60	OHMM	Array Induction One Foot Resistivity A60
AO90	OHMM	Array Induction One Foot Resistivity A90
AORT	OHMM	Array Induction One Foot Rt
AORX	OHMM	Array Induction One Foot Rxo
ASFI	MV	Array Induction SP Filtered
ASN	MV	Amplified Short Normal
AT10	OHMM	Array Induction Two Foot Resistivity A10
AT20	OHMM	Array Induction Two Foot Resistivity A20
AT30	OHMM	Array Induction Two Foot Resistivity A30
AT60	OHMM	Array Induction Two Foot Resistivity A60
AT90	OHMM	Array Induction Two Foot Resistivity A90
ATCO	MM/M	Array Induction Two Foot Conductivity
BED	Cps	
BFV	CFCF	Bound Fluid Volume
BRD		
C1	IN	Caliper 1
C2	IN	Caliper 2
CALI		Caliper
CBP1	CFCF	CMR Bin Porosity 1
CBP2	CFCF	CMR Bin Porosity 2
CBP3	CFCF	CMR Bin Porosity 3
CBP4	CFCF	CMR Bin Porosity 4
CBP5	CFCF	CMR Bin Porosity 5
CBP6	CFCF	CMR Bin Porosity 6

CBP7	CFCF	CMR Bin Porosity 7
CBP8	CFCF	CMR Bin Porosity 8
CDF	LBF	Calibrated Downhole Force
CFTC	HZ	Corrected Far Thermal Counting Rate
CILD	OHMM	Deep Induction Standard Processed Conductivity
CLLR		Collar Locator
CMFF	CFCF	CMR Free Fluid
CMFF_SIG	CFCF	Standard Deviation of CMR Free Fluid
CMRP_3MS	CFCF	CMR 3ms Porosity
CMR_PHI_CONV		CMR Porosity Conversion factor
CNC	G/CC	
CNTC	HZ	Corrected Near Thermal Counting Rate
CORR	G/CC	Correlation Log
CTEM	DEGF	Cartridge Temperature
DCAL		Differential Caliper
DEPT	FT	Depth in Feet
DEVI	DEG	Hole Deviation
DEVIM	DEG	Memorized Deviation
DNPH	CFCF	Delta Thermal Neutron Porosity
DPH8	CFCF	HRDD High Resolution Density Porosity
DPHI	%	Density Porosity
DPHI_1	%	Density Porosity
DPHZ	CFCF	HRDD Standard Resolution Density Porosity
DSOZ	IN	HRDD Standard Resolution Density Stand
DT	*u*sec	Delta-T
DTCO	*u*S/F	Delta-T Compressional
DTSM	*u*S/F	Delta-T Shear
ECGR	GAPI	Environmentally Corrected Gamma-Ray
ECST	DEGF	ECS Temperature
ED	F	East Departure
GDEV	DEG	HGNS Deviation
GR	GAPI	Gamma Ray
GR_1	GAPI	Gamma Ray
GR_2	GAPI	Gamma Ray
GR_3	MMHO	Gamma Ray
GR_EDTC	GAPI	EDTC Gamma Ray
GTEM	DEGF	Generalized Borehole Temperature
HAZI	DEG	Hole Azimuth
HAZIM	DEG	Hole Azimuth
HCAL	IN	HRCC Cal. Caliper

HDPH_SAN	CFCF	HiRes Density Porosity (matrix Sandstone
HDRA	G/C3	HRDD Density Correction
HDRB	G/C3	HRDD Backscatter Delta Rho
HGR	GAPI	HiRes Gamma-Ray
HMIN	OHMM	MCFL Micro Inverse Resistivity
HMNO	OHMM	MCFL Micro Normal Resistivity
HNPO	CFCF	HiRes Enhanced Thermal Neutron Porosity
HPRA		HRDD Photoelectric Factor Correction
HTNP	CFCF	HiRes Thermal Neutron Porosity
HTNP_SAN	CFCF	HiRes Thermal Neutron Porosity
ILD	OHMM	Deep Induction Standard Processed Resist.
ILD_1	OHMM	Deep Induction Standard Processed Resist.
ILD_2	OHMM	Deep Induction Standard Processed Resist.
ILM		Medium Induction Standard Processed Resist.
ITT	S	Integrated Transit Time
KSDR	MD	Permeability from CMR - SDR Model
KTIM	MD	Permeability from CMR - Timur Model
ND	F	North Departure
NEUT	GAPI	Neutrons
NPHI	%	Neutron Porosity
NPOR	CFCF	Enhanced Thermal Neutron Porosity
P1AZ	DEG	Pad 1 Azimuth
P1AZ_GPIT	DEG	Memorized P1AZ
PEF		Photo-Electric Factor
PEF8		HRDD High Resolution Formation Photoelec.
PEFZ		HRDD Standard Resolution Formation Photo
PHIA		Average Porosity
PR		Poisson's Ratio
PXND_HILT	CFCF	HILT Porosity CrossPlot
QCPMT		Photomultiplier Tube Quality Control
RB	DEG	Relative Bearing
RB_GPIT	DEG	Memorized Relative Bearing
RHO8	G/C3	HRDD High Resolution Formation Density
RHOB	G/CC	Bulk Density
RHOZ	G/C3	HRDD Standard Resolution Formation Density
RILD	OHMM	Raw Ild Conductivity
RILD_1	OHMM	Raw Ild Conductivity
RSOZ	IN	MCFL Standard Resolution Resistivity
RWA	OHMM	Apparent Water Resistivity
RWA_HILT	OHMM	HILT Apparent water resistivity

RXO8	OHMM	MCFL High Resolution Invaded Zone Resist
RXOZ	OHMM	MCFL Standard Resolution Invaded Zone Resist.
SDEV	DEG	Sonde Deviation
SDEVM	DEG	Sonde Deviation
SP	Other...	Spontaneous Potential
SPAR	MV	SP Armor Return
SPHI	CFCF	Sonic Porosity
SP_1	MV	Spontaneous Potential
SP_2	Other...	Spontaneous Potential
STIT	F	Stuck Tool Indicator Total
SW		Water Saturation
T2LM	MS	T2 Logarithmic Mean
T2LM_SIG	MS	Standard Deviation of T2 Logarithmic Mea
TCMR	CFCF	Total CMR Porosity
TENS	LBF	Cable Tension
TNPH	CFCF	Thermal Neutron Porosity

APPENDIX III

VOLUMETRIC CALCULATIONS

MT = Megaton; MMSCFD = millions of standard cubic feet per day; MPa = Megapascals; bbl = barrels; S_w = Water Saturation; Vbulk = bulk volume.

	Lower Boyles Sandstone		
	Low	**Median**	**High**
Plant Generation Capacity	1641 MW	1641 MW	1641 MW
Megatons (MT) of CO_2/year at Gorgas	7.5	7.5	7.5
10% of MT CO_2/year	0.75	0.75	0.75
Metric ton per day	2,054.79	2,054.79	2,054.79
MMSCFD per day	38.94	38.94	38.94
Depth (Feet)	1,627.00	1,627.00	1,627.00
Depth (Kilometers)	0.5	0.5	0.5
Temperature of formation Degree C	27.4	27.4	27.4
Pressure of formation MPa	4.96	4.96	4.96
Density of CO_2 at depth (kg/m^3)	120.00	135.00	145.00
Kilograms of CO_2	7,500,000,000.00	7,500,000,000.00	7,500,000,000.00
CO_2 saturation	0.5	0.5	0.5
Porosity (averaged from well logs)	0.06	0.06	0.06
Thickness of formation (meters)	135.33	135.33	135.33
	10 years out	*10 years out*	*10 years out*
Volume occupied by CO_2 (m^3)	62,500,000.00	55,555,555.56	51,724,137.93
Bulk volume of rock saturated with CO_2	2,083,333,333.33	1,851,851,851.85	1,724,137,931.03
Radius (meters) of CO_2 plume	2,214.19	2,087.57	2,014.29
Radius (miles) of CO_2 plume	1.38	1.30	1.25
	20 Years Time	*20 Years Time*	*20 Years Time*
Volume occupied by CO_2	125,000,000.00	111,111,111.11	103,448,275.86
Bulk volume of rock saturated with CO_2	4,166,666,666.67	3,703,703,703.70	3,448,275,862.07
Radius (meters) of CO_2 plume	3,131.34	2,952.27	2,848.64
Radius (miles) of CO_2	1.95	1.83	1.77
	30 Years Time	*30 Years Time*	*30 Years Time*
Volume occupied by CO_2	187,500,000.00	166,666,666.67	155,172,413.79
Bulk volume of rock saturated with CO_2	6,250,000,000.00	5,555,555,555.56	5,172,413,793.10
Radius (meters) of CO_2 plume	3,835.10	3,615.78	3,488.85
Radius (miles) of CO_2 plume	2.38	2.25	2.17
Kilograms of CO_2 injected	22,500,000,000.00	22,500,000,000.00	22,500,000,000.00
Metric tons of CO_2 injected	22,500,000.00	22,500,000.00	22,500,000.00
Megatons of CO_2 injected	22.5	22.5	22.5

VOLUMETRIC CALCULATIONS

MT = Megaton; MMSCFD = millions of standard cubic feet per day; MPa = Megapascals; bbl = barrels; S_w = Water Saturation; Vbulk = bulk volume.

	Hartselle Sandstone		
	Low	**Median**	**High**
Plant Generation Capacity	1641 MW	1641 MW	1641 MW
Megatons (MT) of CO_2/year at Gorgas	7.5	7.5	7.5
10% of MT CO_2/year	0.75	0.75	0.75
Metric ton per day	2,054.79	2,054.79	2,054.79
MMSCFD per day	38.94	38.94	38.94
Depth (Feet)	2,615.00	2,615.00	2,615.00
Depth (Kilometers)	0.8	0.8	0.8
Temperature of formation Degree C	34.93	34.93	34.93
Pressure of formation MPa	7.97	7.97	7.97
Density of CO_2 at depth (kg/m^3)	365.00	400.00	460.00
Kilograms of CO_2	7,500,000,000.00	7,500,000,000.00	7,500,000,000.00
CO_2 saturation	0.5	0.5	0.5
Porosity (averaged from well logs)	0.050104046	0.050104046	0.050104046
Thickness of formation (meters)	26.52	26.52	26.52
	10 years out	*10 years out*	*10 years out*
Volume occupied by CO_2 (m^3)	20,547,945.21	18,750,000.00	16,304,347.83
Bulk volume of rock saturated with CO_2	820,211,010.74	748,442,547.30	650,819,606.35
Radius (meters) of CO_2 plume	3,138.56	2,998.11	2,795.75
Radius (miles) of CO_2 plume	1.95	1.86	1.74
	20 Years Time	*20 Years Time*	*20 Years Time*
Volume occupied by CO_2	41,095,890.41	37,500,000.00	32,608,695.65
Bulk volume of rock saturated with CO_2	1,640,422,021.48	1,496,885,094.60	1,301,639,212.70
Radius (meters) of CO_2 plume	4,438.60	4,239.97	3,953.79
Radius (miles) of CO_2	2.76	2.63	2.46
	30 Years Time	*30 Years Time*	*30 Years Time*
Volume occupied by CO_2	61,643,835.62	56,250,000.00	48,913,043.48
Bulk volume of rock saturated with CO_2	2,460,633,032.22	2,245,327,641.90	1,952,458,819.04
Radius (meters) of CO_2 plume	5,436.15	5,192.88	4,842.38
Radius (miles) of CO_2 plume	3.38	3.23	3.01
Kilograms of CO_2 injected	22,500,000,000.00	22,500,000,000.00	22,500,000,000.00
Metric tons of CO_2 injected	22,500,000.00	22,500,000.00	22,500,000.00
Megatons of CO_2 injected	22.5	22.5	22.5

VOLUMETRIC CALCULATIONS

MT = Megaton; MMSCFD = millions of standard cubic feet per day; MPa = Megapascals; bbl = barrels; S_w = Water Saturation; Vbulk = bulk volume.

	Tuscumbia Limestone		
	Low	**Median**	**High**
Plant Generation Capacity	1641 MW	1641 MW	1641 MW
Megatons (MT) of CO_2/year at Gorgas	7.5	7.5	7.5
10% of MT CO_2/year	0.75	0.75	0.75
Metric ton per day	2,054.79	2,054.79	2,054.79
MMSCFD per day	38.94	38.94	38.94
Depth (Feet)	2,888.00	2,888.00	2,888.00
Depth (Kilometers)	0.88	0.88	0.88
Temperature of formation Degree C	37.01	37.01	37.01
Pressure of formation MPa	8.8	8.8	8.8
Density of CO_2 at depth (kg/m^3)	500.00	515.00	525.00
Kilograms of CO_2	7,500,000,000.00	7,500,000,000.00	7,500,000,000.00
CO_2 saturation	0.5	0.5	0.5
Porosity (averaged from well logs)	0.020706767	0.020706767	0.020706767
Thickness of formation (meters)	60.96	60.96	60.96
	10 years time	*10 years time*	*10 years time*
Volume occupied by CO_2 (m^3)	15,000,000.00	14,563,106.80	14,285,714.29
Bulk volume of rock saturated with CO_2	1,448,801,742.92	1,406,603,633.90	1,379,811,183.73
Radius (meters) of CO_2 plume	2,751.17	2,710.81	2,684.87
Radius (miles) of CO_2 plume	1.71	1.68	1.67
	20Years Time	*20Years Time*	*20Years Time*
Volume occupied by CO_2	30,000,000.00	29,126,213.59	28,571,428.57
Bulk volume of rock saturated with CO_2	2,897,603,485.84	2,813,207,267.80	2,759,622,367.47
Radius (meters) of CO_2 plume	3,890.74	3,833.66	3,796.97
Radius (miles) of CO_2	2.42	2.38	2.36
	30 Years Time	*30 Years Time*	*30 Years Time*
Volume occupied by CO_2	45,000,000.00	43,689,320.39	42,857,142.86
Bulk volume of rock saturated with CO_2	4,346,405,228.76	4,219,810,901.71	4,139,433,551.20
Radius (meters) of CO_2 plume	4,765.16	4,695.26	4,650.32
Radius (miles) of CO_2 plume	2.96	2.92	2.89
Kilograms of CO_2 injected	22,500,000,000.00	22,500,000,000.00	22,500,000,000.00
Metric tons of CO_2 injected	22,500,000.00	22,500,000.00	22,500,000.00
Megatons of CO_2 injected	22.5	22.5	22.5

VOLUMETRIC CALCULATIONS

MT = Megaton; MMSCFD = millions of standard cubic feet per day; MPa = Megapascals; bbl = barrels; S_w = Water Saturation; Vbulk = bulk volume.

	Stones River Group		
	Low	**Median**	**High**
Plant Generation Capacity	1641 MW	1641 MW	1641 MW
Megatons (MT) of CO_2/year at Gorgas	7.5	7.5	7.5
10% of MT CO_2/year	0.75	0.75	0.75
Metric ton per day	2,054.79	2,054.79	2,054.79
MMSCFD per day	38.94	38.94	38.94
Depth (Feet)	3,467.00	3,467.00	3,467.00
Depth (Kilometers)	1.06	1.06	1.06
Temperature of formation Degree C	41.42	41.42	41.42
Pressure of formation MPa	10.57	10.57	10.57
Density of CO_2 at depth (kg/m^3)	545.00	550.00	560.00
Kilograms of CO_2	7,500,000,000.00	7,500,000,000.00	7,500,000,000.00
CO_2 saturation	0.5	0.5	0.5
Porosity (averaged from well logs)	0.006319923	0.006319923	0.006319923
Thickness of formation (meters)	79.55	79.55	79.55
	10 years out	*10 years out*	*10 years out*
Volume occupied by CO_2 (m^3)	13,761,467.89	13,636,363.64	13,392,857.14
Bulk volume of rock saturated with CO_2	4,354,947,704.48	4,315,357,270.80	4,238,297,319.53
Radius (meters) of CO_2 plume	4,175.41	4,156.39	4,119.11
Radius (miles) of CO_2 plume	2.59	2.58	2.56
	20 Years Time	*20 Years Time*	*20 Years Time*
Volume occupied by CO_2	27,522,935.78	27,272,727.27	26,785,714.29
Bulk volume of rock saturated with CO_2	8,709,895,408.95	8,630,714,541.60	8,476,594,639.07
Radius (meters) of CO_2 plume	5,904.92	5,878.02	5,825.30
Radius (miles) of CO_2	3.67	3.65	3.62
	30 Years Time	*30 Years Time*	*30 Years Time*
Volume occupied by CO_2	41,284,403.67	40,909,090.91	40,178,571.43
Bulk volume of rock saturated with CO_2	13,064,843,113.43	12,946,071,812.40	12,714,891,958.60
Radius (meters) of CO_2 plume	7,232.02	7,199.07	7,134.50
Radius (miles) of CO_2 plume	4.49	4.47	4.43
Kilograms of CO_2 injected	22,500,000,000.00	22,500,000,000.00	22,500,000,000.00
Metric tons of CO_2 injected	22,500,000.00	22,500,000.00	22,500,000.00
Megatons of CO_2 injected	22.5	22.5	22.5